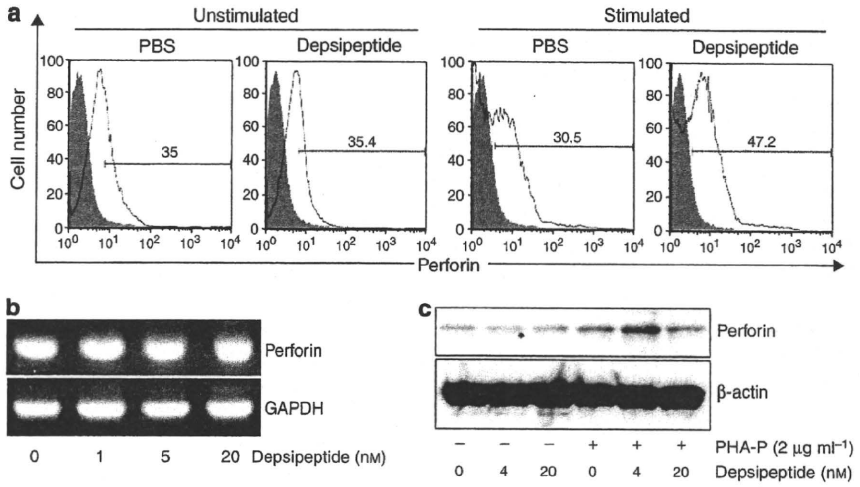

Figure 6. Effect of depsipeptide on perforin expression in effector T cells. (**a**) Increase of perforin-expressing antigen-stimulated pmel-1 T cells by exposure to depsipeptide (5 nM). Primary or antigen-stimulated Pmel-1 T cells (Thy1.1$^+$) with or without depsipeptide (5 nM) for 16 hours were stained by FITC-conjugated anti-mouse perforin mAb after treatment with a Fixation & Permeabilization Kit (eBioscience). Shaded area represents isotype-matched control staining. (**b**) Antigen-stimulated Pmel-1 T cells were treated with depsipeptide at various concentrations for 16 hours, and then perforin mRNA was analyzed by RT-PCR (glyceraldehyde-3-phosphate dehydrogenase (GAPDH), an internal control). (**c**) Human CD8$^+$ T cells were purified from peripheral blood mononuclear cells of healthy volunteers by magnetic bead selection and stimulated with or without PHA-P (2 μg ml^{-1}) *in vitro* for 24 hours. Cells were then lysed and probed for perforin and actin (as an internal control) by western blotting.

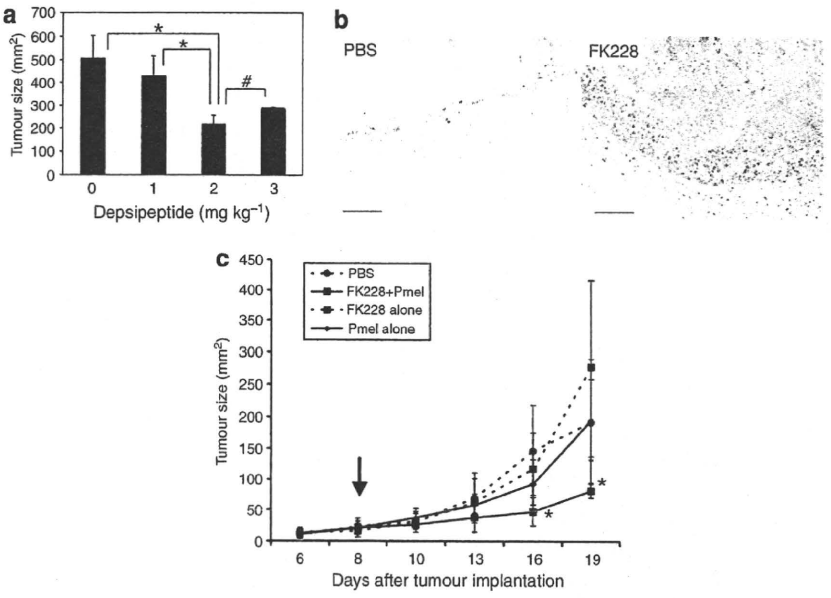

Figure 7. A limited dose of depsipeptide enhances CTL-mediated Luc-B16/F10 cell killing *in vivo*. (**a**) Effect of depsipeptide on B16/F10 tumor growth *in vivo*. B16/F10 cells (1×10^6) were inoculated subcutaneously into the abdominal skin of mice (day 0). A visible tumor in each mouse was established at day 7 after tumor implantation (average size: $122 \pm 20\,mm^2$), and mice were randomized and divided into four groups before treatment. Depsipeptide was administered intraperitoneally into mice from days 7–9 (only for 3 days) at the indicated dose, and activated Pmel-T cells (4×10^6) were subsequently injected intravenously into the tail vein of mice. Tumor growth was measured at day 21 after tumor implantation. The error bars represent the mean ± SD ($n = 4$). $^*P < 0.05$; $^\#P > 0.3$ (Mann–Whitney *U*-test). (**b**) Effect of depsipeptide on histone deacetylation in a subcutaneous tumor of B16/F10 cells. Established B16/F10 skin tumors 1 day after the final depsipeptide administration (2 mg kg^{-1}) were probed for acetyl-histone H3 (Lys 18) by immunohistochemistry (Bar = 100 μm). (**c**) Depsipeptide enhances CTL-mediated B16/F10 tumor killing *in vivo*. B16/F10 cells (5×10^5) were inoculated subcutaneously into the abdominal skin of mice (day 0). A visible tumor in each mouse was established at day 5 after tumor implantation. Depsipeptide (2 mg kg^{-1}) was administered intraperitoneally into mice from days 6–8 (for 3 days), and Pmel-1 CTLs (4×10^6) were subsequently injected intravenously into the tail vein of mice (indicated by the arrow). Tumor growth was monitored every 2–3 days after tumor implantation. The error bars represent the mean ± SD ($n = 5$–6). $^*P < 0.05$ (Kruskal–Wallis test; at days 16 and 19 after tumor implantation). One of three independent experiments with similar results is shown.

of gp100/pmel17 was also observed by RT-PCR assay (Figure S3b). Thus, these data demonstrate that a limited dose of depsipeptide ($2\,mg\,kg^{-1}$) sufficiently sensitized B16/F10 cells *in vivo* for adoptive immunotherapy. Regarding the perforin modulation, we could not determine whether perforin induction occurred *in vivo* by FACS analysis.

We further investigated whether s.c. tumor growth of B16/F10 cells could be inhibited by the adoptive transfer of Pmel-1 CTLs in combination with depsipeptide (Figure 7c). After waiting about a week for tumor growth, $2\,mg\,kg^{-1}$ of depsipeptide was administered via the intra-peritoneal route, followed by the adoptive transfer of Pmel-1 CTLs. In contrast to either CTL transfer alone or depsipeptide pretreatment alone, this combinatorial treatment strikingly suppressed B16/F10 tumor growth. Moreover, we examined whether the above depsipeptide pretreatment and a similar CTL transfer could suppress metastatic tumor growth (Figure 8). Luc-B16/F10 cells were intravenously injected into the tail vain of C57BL/6 mice, and pulmonary metastasis of luc-B16/F10 cells was monitored through luciferase-based luminescent imaging. After waiting about a week for tumor growth, animals were treated with $2\,mg\,kg^{-1}$ of depsipeptide for 3 days, followed by the adoptive transfer of CTLs, which were generated by immunization using irradiated IL-12/IL-18-transduced B16/F10 cells. This combinatorial treatment significantly suppressed tumor-derived photons in pulmonary metastases 21 days following tumor injection. Similar suppression of pulmonary metastases was obtained by adoptive transfer of Pmel-1-derived CTLs (data not shown). Thus, these results demonstrate that sensitization using a limited dose of depsipeptide increases the efficacy of adoptive immunotherapy for established tumors.

DISCUSSION

Cellular unresponsiveness of solid tumor through aberrant transcriptional regulation represents a critical barrier that limits the therapeutic potential of adoptively transferred autologous CTLs in patients with cancer. Herein, we have demonstrated that tumor sensitization with depsipeptide is effective for adoptive immunotherapy against murine B16/F10 melanoma. The remarkable features presented in this study include the following: (1) depsipeptide upregulated gp100/pmel17 melanoma antigen; (2) a limited dose of depsipeptide was able to sufficiently sensitize B16/F10 cells for Fas-mediated apoptosis; (3) depsipeptide increased the perforin-expressing CTLs in post-transcriptional levels; and (4) adoptive cell transfer in combination with depsipeptide led to effective tumor growth suppression.

Emerging evidence suggests that there are a variety of factors that limit tumor regression in the host–tumor interaction. For example, cancer progression often takes place despite the presence of circulating cancer-specific CTLs. Even with patients in whom large numbers of highly activated tumor-specific CTLs have been infused, clinical improvement has been difficult to achieve (Dudley *et al.*, 2001; Rosenberg, 2004). For example, recent evidence concerning host factors suggests that regulatory elements of the immune responses, including $CD4^+CD25^+$ regulatory T cells (Tregs), inhibit the ability of CTLs to produce effective antitumor responses (Antony and Restifo, 2005; Dannull *et al.*, 2005). In regard to tumor-escape factors, many aggressive tumors do not express the tumor antigen or MHC (HLA) antigen (Ferrone and Marincola, 1995; Cabrera *et al.*, 2003). Moreover, many cancer types lack sufficient apoptotic cell death pathways through the aberrant transcription (Johnstone *et al.*, 2002; Maecker *et al.*, 2002). It is theoretically essential to overcome these tumor-escape factors for efficient cancer immunotherapy, and perhaps to manipulate the tumor, as well as the host, before adoptive immune cell transfer.

HDACs are considered among the most promising targets in drug development for cancer, and some HDACi, including depsipeptide (FK228), are currently being tested in phase I and II clinical trials (Minucci and Pelicci, 2006). HDACi is capable of inducing varying degrees of growth arrest,

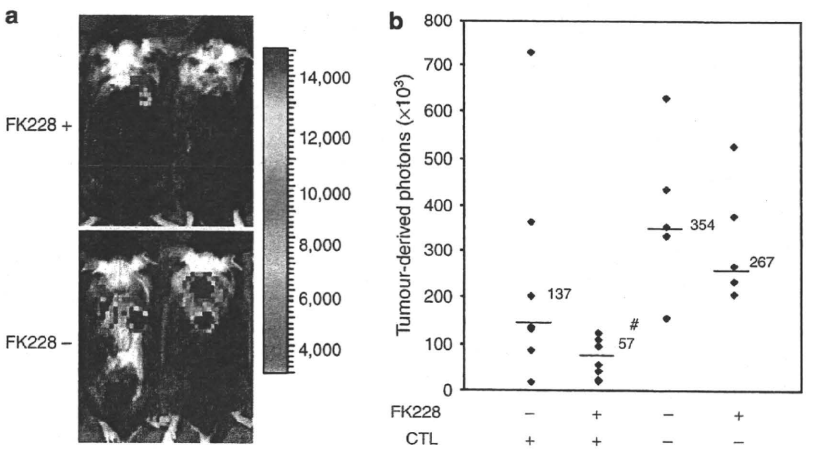

Figure 8. Depsipeptide pretreatment and B16-specific CTLs transfer suppress metastatic tumor growth of B16/F10 cells. (**a**) Representative luciferase images of luc-B16/F10 metastatic lung tumor at day 15 after combinatorial therapy of depsipeptide ($2\,mg\,kg^{-1}$) and immune cell adoptive transfer from immunized mice using irradiated IL-12/IL-18-transduced B16/F10 cells. (**b**) Photon counting of luc-B16/F10-pulmonary metastasis at day 21 ($n=6$–7). $^{\#}P<0.01$ (Kruskal–Wallis test). One of three independent experiments with similar results is shown.

differentiation, or apoptosis of cancer cells (Johnstone *et al.*, 2002; Minucci and Pelicci, 2006). In addition, normal fibroblasts and melanocytes are almost always considerably more resistant than tumor cells to depsipeptide (Kobayashi *et al.*, 2006; Minucci and Pelicci, 2006), suggesting this effect may be specific to malignant cells. We demonstrated the potential upregulation of MHC class I molecules by depsipeptide treatment. As the MHC class I molecule is released from the endoplasmic reticulum only after the peptide has bound and is allowed to reach the cell surface (Williams *et al.*, 2002), this upregulation could provide substantial benefits for the immunological recognition. However, there are abnormalities in the expression and/or function of various components of the MHC class I antigen-processing pathway in human malignant cells (Seliger *et al.*, 2000; Chang and Ferrone, 2007), and it remains to be elucidated whether HDACi affects various components of the protein-processing machinery.

Although the clinical use of depsipeptide when administered alone showed partial and complete responses in patients with hematological malignancy (Piekarz *et al.* 2001, 2004; Byrd *et al.*, 2005), only a partially objective response was observed in solid cancer patients (Sandor *et al.*, 2002; Stadler *et al.*, 2006), suggesting that depsipeptide alone appears far from beneficial in the treatment of cancer patients. However, moving the focus onto the modulation of tumor factors and targeting HDACs could provide great benefits, particularly for selective immunotherapy against cancer. Intriguingly, HDACi could activate components of death receptor pathways, including FasL and tumor necrosis factor-related apoptosis-inducing ligand (TRAIL) (Nakata *et al.*, 2004; Singh *et al.*, 2005; Earel *et al.*, 2006). In fact, B16/F10 cells are less immunogenic and highly resistant to a variety of apoptotic stimuli if they are not manipulated (Avent *et al.*, 1979; Tsai *et al.*, 1997; Kalechman *et al.*, 1998). Nonetheless, exposure of B16 cells to a limited dose of depsipeptide induced cell surface expression of Fas and MHC class I, and the enforced Fas-engagement synergistically increased caspase-3/7 activity of B16/F10 cells in the presence of depsipeptide (Figure 3). Furthermore, these changes successfully provided CTLs with an enhanced ability to recognize and destroy target tumor cells (Figures 4 and 5).

Indeed, it has been demonstrated that HDACi synergizes with exogenously added TRAIL to induce apoptosis of various human solid tumor cell lines *in vitro* (Inoue *et al.*, 2004; Nakata *et al.*, 2004; Singh *et al.*, 2005; Lundqvist *et al.*, 2006). While the TRAIL system seems to be relatively major in the effect of HDACi on the human death receptor pathway, it has been suggested that the effect of HDACi on the death receptor pathway may not be universal (Minucci and Pelicci, 2006). We could not obtain a synergistic effect of depsipeptide with FasL in Fas-negative human MM-LH cells, and mouse Pmel-1 T cells did not express TRAIL on the cell surface (unpublished data). The Fas–FasL system is well known as the major pathway of CTL-mediated tumor destruction in murine models (Kagi *et al.*, 1994; Caldwell *et al.*, 2003; Lee *et al.*, 2006), and therefore some differences between species should be considered for the major death receptor pathway. However, current animal studies have demonstrated that the augmented tumoricidal effects of tumor-specific CTLs induced as a consequence of depsipeptide sensitization resulted in melanoma cells that produced CTL-mediated cytotoxicity *in vivo*. A limited administration of depsipeptide also sufficiently modulated the acetylation level of histone H3 at the tumor site (Figure 7b). These findings may provide the rationale for protocols that pretreat cancer patients with depsipeptide to potentiate adoptive immune therapy.

Emerging experimental data indicate that lymphodepletion using cyclophosphamide before adoptive transfer of tumor-specific T lymphocytes plays a key role in enhancing treatment efficacy by eliminating regulatory T cells and competing elements of the immune system (Ghiringhelli *et al.*, 2004; Lutsiak *et al.*, 2005). Furthermore, pretreatment with cyclophosphamide contributes to the elimination of immunosuppressive cells such as $CD4^+CD25^+$ Treg in patients with cancer and the depletion of endogenous cells that compete for the activation of cytokines (known as the "cytokine sink") to maximize the exposure of homeostatic cytokines to the transferred CTLs (Gattinoni *et al.*, 2006). In addition to this pretreatment, depsipeptide may safely be added to reduce barrier tumor factors limiting the therapeutic potential of adoptively transferred CTLs. We further demonstrated that depsipeptide increased the level of perforin in activated T cells to varying degrees: the number of perforin-expressing CTLs increased in mice, whereas an accumulation of perforin was observed in humans. Perforin release by T cells in conjunction with granzymes induces an apoptotic cascade in target cells (Kagi *et al.*, 1994). In fact, Palmer *et al.* (2004) showed that there was a B16 cell-dependent release of perforin after adoptive cell transfer of pmel-1 T cells, in which caspase-3 activation was also shown at the tumor site as a consequence of the downstream activation of perforin. Therefore, the residual depsipeptide in the plasma of pretreated hosts could be expected to release large amounts of toxic granules to the target tumor at the sites and, in combination with cyclophosphamide, the use of depsipeptide may be considered for host and tumor modulation before adoptive tumor-specific CTL transfer.

The therapeutic options for patients with metastatic disease remain limited, and the majority of these patients will develop a local or systemic recurrence. A variety of human cancers such as melanoma and breast, colon, and prostate cancers aberrantly express the chemokine receptor CXCR4 (Balkwill, 2004; Kakinuma and Hwang, 2006; Zlotnik, 2006), and its activation through prosurvival pathways such as Akt has been implicated as a mechanism by which cancer cells evade host immunity (Murakami *et al.*, 2003) and increase their metastatic properties (Kakinuma and Hwang, 2006). Recently, Lee *et al.* (2006) reported that sensitization of B16 cells with a CXCR4 antagonistic peptide increases the efficacy of immunotherapy for pulmonary metastases, suggesting that the inhibition of tumor factor is an effective strategy for melanoma immunotherapy. Herein, we also provide compelling *in vitro* and *in vivo* data suggesting that sensitization of less immunogenic B16 cells with depsipeptide facilitates the efficacy of immunotherapy

for established pulmonary metastases. Further investigations based on the findings of this study, especially those incorporating *in vivo* techniques, should improve the design of optimized clinical protocols.

MATERIALS AND METHODS

Animals, cells, and reagents

Male C57BL/6J mice (8–12 weeks old) were purchased from Charles River Japan Inc. (Tsukuba, Japan). Pmel-1 TCR pmel-1 +/Thy1.1 + transgenic mice (Overwijk *et al.*, 2003) were obtained from The Jackson Laboratory (Bar Harbor, ME). All experiments in this study were approved by the animal ethics review board of Jichi Medical University and performed in accordance with the Jichi Medical University Guide for Laboratory Animals, following the principles of laboratory animal care formulated by the National Society for Medical Research.

Human melanoma cell lines RPM-MC, MM-LH, MM-BP, and MM-RU were kindly provided by Dr H. Randolph Byers (Boston University Medical School) and maintained in minimal essential medium supplemented with 10% heat-inactivated fetal calf serum (FCS) (Byers *et al.*, 1991). Murine B16/F10 melanoma cells (Fidler, 1973) and EL-4 thymoma cells (Ralph, 1973) were grown in DMEM (GIBCO, Gaithersburg, MD) with 10% FCS and supplements (Sato *et al.*, 2006). Luciferase-expressing B16/F10 (luc-B16/F10) cells were generated previously (Sato *et al.*, 2006) and maintained in DMEM with 10% FCS and supplements, including puromycin (10 $\mu g\,ml^{-1}$; Sigma-Aldrich, St Louis, MO). Normal human epidermal melanocytes were purchased from Kurabo Biomedicals (Osaka, Japan) and maintained in Medium 154S with supplement (Kobayashi *et al.*, 2006). The cultures were kept in a humidified atmosphere containing 5% CO_2 and 95% air at 37°C.

Anti-acetyl-histone H3 (Lys 9), anti-acetyl-histone H3 (Lys 18), anti-histone H3, and anti-phospho-Rb (Ser 780) antibodies were purchased from Cell Signaling Technology (Beverly, MA). Anti-mouse $p21^{Waf1/Cip1}$ (BD Pharmingen, San Diego, CA), anti-human perforin (clone δG9; BD Pharmingen), and anti-actin (sc-1616, Santa Cruz Biotechnology Inc., Santa Cruz, CA) antibodies were used for western blotting. Flow cytometric analysis involved the use of phycoerythrin (PE)-conjugated anti-mouse $H\text{-}2D^b$ mAb, PE-conjugated anti-mouse Fas (CD95) mAb, PE-conjugated anti-mouse FasL (CD178) mAb, and isotype-matched IgG controls, all of which were purchased from BD Pharmingen. FITC-conjugated anti-mouse perforin mAb (clone: eBioOMAK-D) was purchased from eBioscience (San Diego, CA). Anti-mouse FasL mAb (clone MFL3; BD Pharmingen) was used for the FasL neutralization.

The expression plasmids for mouse IL-12 and IL-18, pCAGGS-IL-12 and pcDNA-mproIL-18-mICE respectively, have been described previously (Ajiki *et al.*, 2003). Depsipeptide (FK228) was obtained from Gloucester Pharmaceuticals (Cambridge, MA).

Reverse transcription-PCR

Total RNA was extracted from cells using Isogen (Nippon Gene, Toyama, Japan). Two micrograms of total RNA was used for first-strand synthesis using SuperScript III reverse transcriptase (Invitrogen, Carlsbad, CA). PCR was then performed using ExTaq polymerase (Takara, Ohtsu, Japan). The following primers were used for gp100/pmel-17 and perforin expression analysis: human gp100/pmel-17 sense, 5′-CCTCCTTCTCTATTGCCTTG-3′; human gp100/pmel-17 anti-sense, 5′-TGTAGGAGAGGTGAGCTTCA-3′; mouse gp100 sense, 5′-GGCCAACAACACCATCATCA-3′; mouse gp100 anti-sense, 5′-GGGCAAAGATGAGAGGATGA-3′; mouse perforin sense, 5′-ACAATAACAATCCCCGGTGG-3′; mouse perforin anti-sense, 5′-TGGGATTAAAGGCGTGTGCT-3′; glyceraldehyde-3-phosphate dehydrogenase sense, 5′-GTATCGTGGAAGGACTCATG-3′; and glyceraldehyde-3-phosphate dehydrogenase anti-sense, 5′-AGT GGGTGTCGCGCTGTTGAAG-3′. PCR conditions for each set of primers included an initial treatment at 95°C for 2 minutes, followed by 30 cycles consisting of denaturation at 95°C for 15 seconds, annealing at 57°C for 30 seconds, and then extension at 72°C for 2 minutes. PCR products were analyzed using a 1% agarose gel.

Transfection and ELISA

B16/F10 cells (1×10^6) were transfected with pCAGGS-IL-12 (5 μg) and pcDNA-mproIL-18-mICE (5 μg) using Lipofectamine 2000 (Invitrogen). Immunization experiments involved irradiating IL-12/IL-18-transfected B16 cells with 80 Gy 36 hours after transfection. Irradiated cells ($1\text{–}2 \times 10^5$) were then injected twice into the subcutaneous space of C57BL/6 mice during the remaining weeks.

To analyze IFN-γ production, splenocytes ($1\text{–}2 \times 10^5$) that were isolated from immunized mice were co-cultured for 24 hours with 1×10^5 irradiated target cells, and the IFN-γ concentration of supernatants was then measured using a mouse IFN-γ immunoassay kit. All samples were assayed in triplicate.

Apoptosis and cytotoxic assay

To detect caspase-3/7 activity, B16/F10 cells (2×10^4 per well of a 96-well plate) were plated, and the Caspase-Glo 3/7 Assay system (Promega, Madison, WI) was used for analysis in accordance with the manufacturer's instructions 16 hours after the addition of depsipeptide. The background luminescence associated with the cell culture and assay reagent (blank reaction) was subtracted from experimental values. Means of triplicates were used to represent caspase-3/7 activity for the given cells. Each experiment was performed three times with similar results.

For enhancement of Fas-mediated apoptosis, B16/F10 cells were exposed to 10 $ng\,ml^{-1}$ recombinant human FLAG-tagged FasL (Apotech, San Diego, CA) in combination with 1 $mg\,ml^{-1}$ anti-FLAG M2 mAb (Sigma, St Louis, MO) for 16 hours with 5 nM depsipeptide at 37°C in the presence of 0.5% FCS, as described previously (Murakami *et al.*, 2003). After exposure of B16/F10 cells to apoptosis-enhancing conditions for 16 hours, attached (and detached) cells were collected from tissue culture plates for annexin-V staining according to the manufacturer's instructions (MEBCYTO Apoptosis Kit; MBL, Nagoya, Japan). Analysis of caspase-3/7 activity involved the assessment of 2×10^4 cells using the Caspase-Glo 3/7 Assay system (Promega).

Western blotting and flow cytometry

For western blotting, cells were lysed by sonication in radio-immuno-protein assay (RIPA) buffer (Sato *et al.*, 2006) and then centrifuged for 10 minutes at 4°C. Each cell extract (10 μg of protein) was assayed using appropriate antibodies and protein G-conjugated horseradish peroxidase (Amersham Pharmacia Biotech, Buckinghamshire, UK).

For the flow cytometric analysis, cells (1×10^6) were washed with phosphate buffered saline (PBS) and incubated with mAb for

30 minutes at 4°C. Following washing with 0.1% FCS-PBS, cells were analyzed using FACS Calibur (Becton Dickinson, Mountain View, CA) and FlowJo analysis software (Tree Star, San Carlos, CA).

Subcutaneous and intravenous tumor inoculation

Cells in an exponential growth phase were harvested by trypsinization and washed twice in PBS before injection. For the s.c. injections, cells (1×10^6) were injected into the abdominal subcutaneous space of C57BL/6 mice. Tumor growth at the skin was monitored by measurement of the two maximum perpendicular tumor diameters. For the intravenous injections to the lungs, luc-B16/F10 cells (5×10^4 in 0.2 ml PBS) were injected into the tail vein of C57BL/6 mice. Each experiment was performed 2–4 times with similar results.

In vivo bioluminescence imaging

In vivo tumor progression was examined using the noninvasive bioimaging system IVIS (Xenogen, Alameda, CA). Tumor-implanted mice were anesthetized with a mixture of ketamine and xylazine, and D-luciferin (potassium salt; Biosynth, Postfach, Switzerland) was injected into the peritoneal cavity at 2 mg per animal, which was followed immediately by the measurement of luciferase activity. The imaging system consisted of a cooled, back-thinned charge-coupled device camera to capture both a visible light photograph of the animal taken with light-emitting diodes and a luminescent image. After acquiring photographic images of each mouse, luminescent images were acquired with a 1–15 minutes exposure time (Ohsawa *et al.*, 2006; Sato *et al.*, 2006). Images were obtained with a 25 cm field of view, a binning (resolution) factor of 8, 1/f stop, and an open filter. The resulting gray scale photographic and pseudo-color luminescent images were automatically superimposed by software to facilitate the identification of any optical signal and the location on the mouse. Optical images were displayed and analyzed using Igor (WaveMetrics, Lake Oswego, OR) and IVIS Living Image (Xenogen) software packages. The signal from tumors was quantified as photons flux in units of photons per second per cm^2 per sr.

Immunohistochemistry

Removed specimens were fixed with 10% paraformaldehyde and embedded in paraffin. Tissue sections (5 μm) deparaffinized in xylene were passed through graded alcohols before being treated with 1% H_2O_2 (v/v) in H_2O for 20 minutes at room temperature. After washing the sections three times with PBS, sections were blocked for 20 minutes with 10% FCS diluted in PBS. All incubations were performed at room temperature in a moist chamber. The slides were incubated overnight at 4°C with anti-acetyl-histone H3 (Lys 18) antibody (no. 9675, Cell Signaling Technology) diluted 1:100 in blocking solution. The sections were washed in PBS and incubated with biotinylated goat anti-rabbit secondary antibody (Vector Laboratories, Burlingame, CA), and staining was visualized using a streptavidin-peroxidase conjugate (Vector Laboratories). A diaminobenzidine substrate kit (Vector Laboratories) was used for color (brown) visualization, and sections were counterstained with hematoxylin.

Statistical analysis

P-values based on two-sided Student's *t*-test, Mann–Whitney test, or Kruskal–Wallis test were obtained using the Instat software package (GraphPad, San Diego, CA). Differences between groups were considered significant if $P<0.05$.

CONFLICT OF INTEREST

The authors state no conflict of interest.

ACKNOWLEDGMENTS

We would like to thank Ms Yasuko Sakuma, Ms Yumi Ohde, and Ms Masayo Kumagai for their skillful technical assistance. This study was supported by a grant to T.M. from the Kowa Life Science Foundation (2004) and the Ministry of Education, Culture, Sports, Science and Technology (MEXT) of Japan (Project No. 17591181; 2005–2007) and by a grant from the "High-Tech Research Center" Project for Private Universities: matching fund subsidy from MEXT (2003–2007).

SUPPLEMENTARY MATERIAL

Figure S1. Expression of HLA class I (A, B, C) and Fas (CD95/Apo-1) in human melanoma cell lines following exposure to depsipeptide.

Figure S2. Increase of perforin in PHA-stimulated human T cells by exposure to depsipeptide (4 nM).

Figure S3. Effect of depsipeptide on the subcutaneous tumor of B16/F10 cells.

REFERENCES

Ajiki T, Murakami T, Kobayashi Y, Hakamata Y, Wang J, Inoue S *et al.* (2003) Long-lasting gene expression by particle-mediated intramuscular transfection modified with bupivacaine: combinatorial gene therapy with IL-12 and IL-18 cDNA against rat sarcoma at a distant site. *Cancer Gene Ther* 10:318–29

Antony PA, Restifo NP (2005) CD4+CD25+ T regulatory cells, immunotherapy of cancer, and interleukin-2. *J Immunother* 28:120–8

Avent J, Vervaert C, Seigler HF (1979) Non-specific and specific active immunotherapy in a B16 murine melanoma system. *J Surg Oncol* 12: 87–96

Balkwill F (2004) Cancer and the chemokine network. *Nat Rev Cancer* 4: 540–50

Byers HR, Etoh T, Doherty JR, Sober AJ, Mihm MC Jr (1991) Cell migration and actin organization in cultured human primary, recurrent cutaneous and metastatic melanoma. Time-lapse and image analysis. *Am J Pathol* 139:423–35

Byrd JC, Marcucci G, Parthun MR, Xiao JJ, Klisovic RB, Moran M *et al.* (2005) A phase 1 and pharmacodynamic study of depsipeptide (FK228) in chronic lymphocytic leukemia and acute myeloid leukemia. *Blood* 105:959–67

Cabrera T, Lopez-Nevot MA, Gaforio JJ, Ruiz-Cabello F, Garrido F (2003) Analysis of HLA expression in human tumor tissues. *Cancer Immunol Immunother* 52:1–9

Caldwell SA, Ryan MH, McDuffie E, Abrams SI (2003) The Fas/Fas ligand pathway is important for optimal tumor regression in a mouse model of CTL adoptive immunotherapy of experimental CMS4 lung metastases. *J Immunol* 171:2402–12

Chang CC, Ferrone S (2007) Immune selective pressure and HLA class I antigen defects in malignant lesions. *Cancer Immunol Immunother* 56: 227–36

Dannull J, Su Z, Rizzieri D, Yang BK, Coleman D, Yancey D *et al.* (2005) Enhancement of vaccine-mediated antitumor immunity in cancer patients after depletion of regulatory T cells. *J Clin Invest* 115: 3623–33

Dudley ME, Wunderlich J, Nishimura MI, Yu D, Yang JC, Topalian SL *et al.* (2001) Adoptive transfer of cloned melanoma-reactive T lymphocytes for the treatment of patients with metastatic melanoma. *J Immunother* 24:363–73

Earel JK Jr, VanOosten RL, Griffith TS (2006) Histone deacetylase inhibitors modulate the sensitivity of tumor necrosis factor-related apoptosis-inducing ligand-resistant bladder tumor cells. *Cancer Res* 66: 499–507

Ferrone S, Marincola FM (1995) Loss of HLA class I antigens by melanoma cells: molecular mechanisms, functional significance and clinical relevance. *Immunol Today* 16:487–94

Fidler IJ (1973) Selection of successive tumour lines for metastasis. *Nat New Biol* 242:148–9

Gattinoni L, Powell DJ Jr, Rosenberg SA, Restifo NP (2006) Adoptive immunotherapy for cancer: building on success. *Nat Rev Immunol* 6: 383–93

Ghiringhelli F, Larmonier N, Schmitt E, Parcellier A, Cathelin D, Garrido C *et al.* (2004) $CD4^+CD25^+$ regulatory T cells suppress tumor immunity but are sensitive to cyclophosphamide which allows immunotherapy of established tumors to be curative. *Eur J Immunol* 34:336–44

Herman JG, Baylin SB (2003) Gene silencing in cancer in association with promoter hypermethylation. *N Engl J Med* 349:2042–54

Hoshikawa Y, Kwon HJ, Yoshida M, Horinouchi S, Beppu T (1994) Trichostatin A induces morphological changes and gelsolin expression by inhibiting histone deacetylase in human carcinoma cell lines. *Exp Cell Res* 214:189–97

Inoue S, MacFarlane M, Harper N, Wheat LM, Dyer MJ, Cohen GM (2004) Histone deacetylase inhibitors potentiate TNF-related apoptosis-inducing ligand (TRAIL)-induced apoptosis in lymphoid malignancies. *Cell Death Differ* 11(Suppl 2):S193–206

Johnstone RW, Licht JD (2003) Histone deacetylase inhibitors in cancer therapy: is transcription the primary target? *Cancer Cell* 4:13–8

Johnstone RW, Ruefli AA, Lowe SW (2002) Apoptosis: a link between cancer genetics and chemotherapy. *Cell* 108:153–64

Kagi D, Vignaux F, Ledermann B, Burki K, Depraetere V, Nagata S *et al.* (1994) Fas and perforin pathways as major mechanisms of T cell-mediated cytotoxicity. *Science* 265:528–30

Kakinuma T, Hwang ST (2006) Chemokines, chemokine receptors, and cancer metastasis. *J Leukoc Biol* 79:639–51

Kalechman Y, Strassmann G, Albeck M, Sredni B (1998) Up-regulation by ammonium trichloro(dioxoethylene-0,0′) tellurate (AS101) of Fas/Apo-1 expression on B16 melanoma cells: implications for the antitumor effects of AS101. *J Immunol* 161:3536–42

Klisovic DD, Katz SE, Effron D, Klisovic MI, Wickham J, Parthun MR *et al.* (2003) Depsipeptide (FR901228) inhibits proliferation and induces apoptosis in primary and metastatic human uveal melanoma cell lines. *Invest Ophthalmol Vis Sci* 44:2390–8

Kobayashi Y, Ohtsuki M, Murakami T, Kobayashi T, Sutheesophon K, Kitayama H *et al.* (2006) Histone deacetylase inhibitor FK228 suppresses the Ras-MAP kinase signaling pathway by upregulating Rap1 and induces apoptosis in malignant melanoma. *Oncogene* 25:512–24

Lee CH, Kakinuma T, Wang J, Zhang H, Palmer DC, Restifo NP *et al.* (2006) Sensitization of B16 tumor cells with a CXCR4 antagonist increases the efficacy of immunotherapy for established lung metastases. *Mol Cancer Ther* 5:2592–9

Lundqvist A, Abrams SI, Schrump DS, Alvarez G, Suffredini D, Berg M *et al.* (2006) Bortezomib and depsipeptide sensitize tumors to tumor necrosis factor-related apoptosis-inducing ligand: a novel method to potentiate natural killer cell tumor cytotoxicity. *Cancer Res* 66:7317–25

Lutsiak ME, Semnani RT, De Pascalis R, Kashmiri SV, Schlom J, Sabzevari H (2005) Inhibition of CD4(+)25(+) T regulatory cell function implicated in enhanced immune response by low-dose cyclophosphamide. *Blood* 105:2862–8

Maecker HL, Yun Z, Maecker HT, Giaccia AJ (2002) Epigenetic changes in tumor Fas levels determine immune escape and response to therapy. *Cancer Cell* 2:139–48

Marks P, Rifkind RA, Richon VM, Breslow R, Miller T, Kelly WK (2001) Histone deacetylases and cancer: causes and therapies. *Nat Rev Cancer* 1:194–202

Minucci S, Pelicci PG (2006) Histone deacetylase inhibitors and the promise of epigenetic (and more) treatments for cancer. *Nat Rev Cancer* 6:38–51

Murakami T, Cardones AR, Finkelstein SE, Restifo NP, Klaunberg BA, Nestle FO *et al.* (2003) Immune evasion by murine melanoma mediated through CC chemokine receptor-10. *J Exp Med* 198:1337–47

Nakata S, Yoshida T, Horinaka M, Shiraishi T, Wakada M, Sakai T (2004) Histone deacetylase inhibitors upregulate death receptor 5/TRAIL-R2 and sensitize apoptosis induced by TRAIL/APO2-L in human malignant tumor cells. *Oncogene* 23:6261–71

Ohsawa I, Murakami T, Uemoto S, Kobayashi E (2006) *In vivo* luminescent imaging of cyclosporin A-mediated cancer progression in rats. *Transplantation* 81:1558–67

Overwijk WW, Theoret MR, Finkelstein SE, Surman DR, de Jong LA, Vyth-Dreese FA *et al.* (2003) Tumor regression and autoimmunity after reversal of a functionally tolerant state of self-reactive CD8+ T cells. *J Exp Med* 198:569–80

Palmer DC, Balasubramaniam S, Hanada K, Wrzesinski C, Yu Z, Farid S *et al.* (2004) Vaccine-stimulated, adoptively transferred CD8+ T cells traffic indiscriminately and ubiquitously while mediating specific tumor destruction. *J Immunol* 173:7209–16

Piekarz RL, Robey R, Sandor V, Bakke S, Wilson WH, Dahmoush L *et al.* (2001) Inhibitor of histone deacetylation, depsipeptide (FR901228), in the treatment of peripheral and cutaneous T-cell lymphoma: a case report. *Blood* 98:2865–8

Piekarz RL, Robey RW, Zhan Z, Kayastha G, Sayah A, Abdeldaim AH *et al.* (2004) T-cell lymphoma as a model for the use of histone deacetylase inhibitors in cancer therapy: impact of depsipeptide on molecular markers, therapeutic targets, and mechanisms of resistance. *Blood* 103:4636–43

Ralph P (1973) Retention of lymphocyte characteristics by myelomas and theta+-lymphomas: sensitivity to cortisol and phytohemagglutinin. *J Immunol* 110:1470–5

Rosenberg SA (2004) Shedding light on immunotherapy for cancer. *N Engl J Med* 350:1461–3

Rosenberg SA, Dudley ME (2004) Cancer regression in patients with metastatic melanoma after the transfer of autologous antitumor lymphocytes. *Proc Natl Acad Sci USA* 101(Suppl 2):14639–45

Rosenberg SA, Yang JC, Restifo NP (2004) Cancer immunotherapy: moving beyond current vaccines. *Nat Med* 10:909–15

Sandor V, Bakke S, Robey RW, Kang MH, Blagosklonny MV, Bender J *et al.* (2002) Phase I trial of the histone deacetylase inhibitor, depsipeptide (FR901228, NSC 630176), in patients with refractory neoplasms. *Clin Cancer Res* 8:718–28

Sato A, Ohtsuki M, Hata M, Kobayashi E, Murakami T (2006) Antitumor activity of IFN-lambda in murine tumor models. *J Immunol* 176: 7686–94

Seliger B, Maeurer MJ, Ferrone S (2000) Antigen-processing machinery breakdown and tumor growth. *Immunol Today* 21:455–64

Singh TR, Shankar S, Srivastava RK (2005) HDAC inhibitors enhance the apoptosis-inducing potential of TRAIL in breast carcinoma. *Oncogene* 24:4609–23

Stadler WM, Margolin K, Ferber S, McCulloch W, Thompson JA (2006) A phase II study of depsipeptide in refractory metastatic renal cell cancer. *Clin Genitourin Cancer* 5:57–60

Tsai V, Southwood S, Sidney J, Sakaguchi K, Kawakami Y, Appella E *et al.* (1997) Identification of subdominant CTL epitopes of the GP100 melanoma-associated tumor antigen by primary *in vitro* immunization with peptide-pulsed dendritic cells. *J Immunol* 158: 1796–802

Ueda H, Manda T, Matsumoto S, Mukumoto S, Nishigaki F, Kawamura I *et al.* (1994a) FR901228, a novel antitumor bicyclic depsipeptide produced by Chromobacterium violaceum No. 968. III. Antitumor activities on experimental tumors in mice. *J Antibiot (Tokyo)* 47: 315–23

Ueda H, Nakajima H, Hori Y, Goto T, Okuhara M (1994b) Action of FR901228, a novel antitumor bicyclic depsipeptide produced by Chromobacterium violaceum no. 968, on Ha-ras transformed NIH3T3 cells. *Biosci Biotechnol Biochem* 58:1579–83

Williams A, Peh CA, Elliott T (2002) The cell biology of MHC class I antigen presentation. *Tissue Antigens* 59:3–17

Zlotnik A (2006) Chemokines and cancer. *Int J Cancer* 119:2026–9

Journal of Biomedical Optics 13(6), 064036 (November/December 2008)

Bioimaging assessment and effect of skin wound healing using bone-marrow-derived mesenchymal stromal cells with the artificial dermis in diabetic rats

Hirokazu Inoue
Jichi Medical University
Division of Organ Replacement Research
Center for Molecular Medicine
and
Department of Orthopedics
Tochigi 329-0498, Japan

Takashi Murakami
Jichi Medical University
Division of Organ Replacement Research
Center for Molecular Medicine
Tochigi 329-0498, Japan

Takashi Ajiki
Jichi Medical University
Division of Organ Replacement Research
Center for Molecular Medicine
and
Department of Orthopedics
Tochigi 329-0498, Japan

Mayumi Hara
Jichi Medical University
Division of Organ Replacement Research
Center for Molecular Medicine
Tochigi 329-0498, Japan

Yuichi Hoshino
Jichi Medical University
Department of Orthopedics
Tochigi 329-0498, Japan

Eiji Kobayashi
Jichi Medical University
Division of Organ Replacement Research
Center for Molecular Medicine
Tochigi 329-0498, Japan

Abstract. We investigate the relationship between the fate and healing effect of transplanted mesenchymal stromal cells (MSCs) in a rat diabetic skin wound model. Rats are treated with streptozotocin to induce diabetic conditions. A full-thickness skin defect is surgically made on the head of diabetic rats, and covered with an artificial dermis impregnated with either bone marrow cells (BMCs) or bone-marrow-derived MSCs from firefly luciferase (luc) transgenic (Tg) rats. Wound healing is evaluated using planimetry and immunohistochemistry, and the fate of transplanted MSCs is determined using *in-vivo* luminescent imaging. The diabetic wound treated with MSCs-impregnated artificial dermis is significantly smaller than that treated with artificial dermis alone at 1 week postoperation. Photons of luc+ MSCs are detected at the transplanted site during healing (3 weeks), whereas those of luc+ MSCs are depleted only after 1 week postimplantation. Immunohistochemistry at the healing site treated with MSCs demonstrates that CD31+ vessels increase with expression of vascular endothelial growth factor, suggesting that MSCs accelerate angiogenesis. These findings suggest that transplanted MSCs could be retained at wound sites during the healing process in a diabetic rat model, and subsequently promote wound healing through angiogenesis.
[DOI: 10.1117/1.3042266]

Keywords: wound healing; mesenchymal stromal cell; angiogenesis; bone marrow cell; luminescence.

Paper 08130R received Apr. 20, 2008; revised manuscript received Sep. 14, 2008; accepted for publication Oct. 28, 2008; published online Dec. 18, 2008.

1 Introduction

Impaired wound healing represents a major clinical problem in patients with diabetes. The diabetic ulcer is a chronic and intractable injury, represents one of the most serious complications associated with diabetes, and is a leading cause of lower extremity amputation.[1] The lifetime risk of a person with diabetes developing a foot ulcer could be as high as 25%, and every 30 sec a lower limb is lost somewhere in the world as a consequence of diabetes.[2] Consequently, a novel strategy for the treatment of diabetic wounds is strongly needed to reduce clinical morbidity.[3]

Recently, attention has focused on cell therapy using bone-marrow-derived cells as a treatment of diabetic chronic wounds.[3–5] In fact, therapeutic trials involving bone marrow cells (BMCs) were clinically employed for the treatment of chronic wounds, including diabetic ulcers and decubitus.[3,6,7] Those studies demonstrated that BMCs play a critical role in angiogenesis and vasculogenesis for tissue repair,[8] and that bone-marrow-derived progenitor cells are recruited to peripheral tissues in response to ischemia.[9] In particular, BMCs include mesenchymal stromal cells [or mesenchymal stem cells

Address all Correspondence to: Eiji Kobayashi, M.D., Ph.D., Division of Organ Replacement Research, Center for Molecular Medicine, Jichi Medical University, Yakushiji 3311-1, Shimotsuke, Tochigi 329-0498 Japan. Tel: +81-285-58-7446; Fax: +81-285-44-5365; E-mail: eijikoba@jichi.ac.jp

1083-3668/2008/13(6)/064036/10/$25.00 © 2008 SPIE

(MSCs)], which have been shown to self-renew and differentiate into multilineage cells such as bone, cartilage, fat, myoblasts, vessels, and neurons.[10–17] Bone-marrow-derived MSCs possess a high expansion potential *ex vivo*, genetic stability, and can easily be isolated and transferred from the laboratory to the bedside. Thus, the clinical use of MSCs is of considerable interest in regenerative medicine.

While the use of MSCs offers insights into a new therapeutic approach concerning the repair of diabetic wounds, their fate following tissue implantation remains unclear. To determine the behavior of transplanted cells, an appropriate marker is essential in delineating the scientific basis of preclinical investigations. In this respect, firefly (*Photinus pyralis*) luciferase transgenic rats provide a stable internal light source for examining the behavior of transplanted cells in living rats. Moreover, the larger body size of the rat compared with the mouse allows for various surgical manipulations that may prove to have preclinical significance.

We demonstrate the relationship between the fate and role of bone-marrow-derived MSCs using topical transplantation of MSCs from luciferase transgenic rats to a diabetic skin wound. Our data showed that transplanted MSCs could be sufficiently retained during the healing period at wound sites, and that their retention was well correlated with improved wound healing. Immunohistochemistry also demonstrated that vascular endothelial growth factor and hypoxia-inducible factor 1α were expressed at the healing site treated with MSCs. Thus, these results support the view that the use of bone-marrow-derived MSCs promotes diabetic wound healing through their long retention and expression of angiogenic factors.

2 Experimental Materials and Methods

2.1 *Animals, Antibodies, and Reagents*

Male Lewis (LEW) rats (250 to 280 g) were purchased from Charles River Japan, Incorporated (Yokohama, Japan). LacZ-Tg LEW rats (ROSA/LacZ-LEW)[18,19] and luciferase (luc)-Tg LEW rats (ROSA/Luciferase-LEW)[20] previously generated were used as donors (8 to 12 weeks old). All rats had free access to standard chow and drinking water, and were maintained on a 12-h light/dark cycle. All animal experiments in this study were performed in accordance with the Jichi Medical University Guide for Laboratory Animals.

Fluorescent isothiocyanate (FITC)-conjugated antirat CD29 monoclonal antibody (mAb, clone Ha2/5), (FITC)-conjugated antirat CD90 (Thy-1, clone HIS51) mAb, and phycoerythrin (PE)-conjugated antirat CD45 mAb (clone OX-1) were purchased from BD Pharmingen (San Diego, California). PE-conjugated antirat CD34 mAb (clone ICO115, sc-7324) was purchased from Santa Cruz Biotechnology (Santa Cruz, California). Isotype-matched IgG controls were purchased from BD Pharmingen. Mouse antivascular endothelial growth factor (VEGF) mAb (clone C1, sc-7269, Santa Cruz), rabbit anti-CD31 affinity-purified IgG (sc-1506-R, Santa Cruz), mouse IgG (sc-3879, Santa Cruz), and mouse antihypoxia inducible factor-1α (HIF-1α) mAb (clone, H1alpha67, MAB5382, Chemicon, Temecula, California) were used as the primary Ab for immunohistochemistry, followed by biotinylated antirabbit (BA-1000) and antimouse IgG (BA-2001, Vector Laboratories, Burlingame, California), respectively.

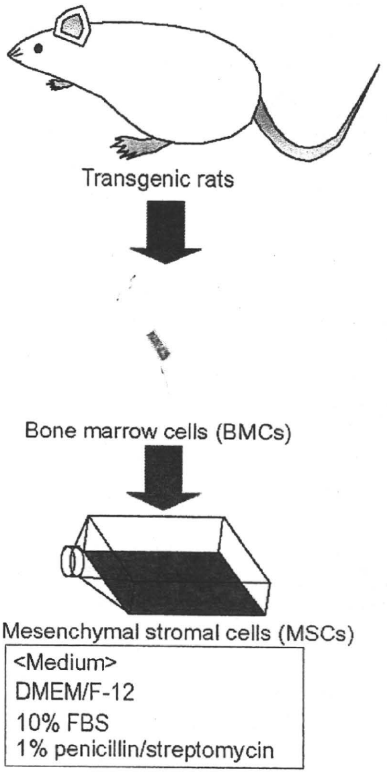

Fig. 1 Schematic of mesenchymal stromal cells (MSCs) purification. Bone marrow cells (BMCs) were harvested by flushing femurs and tibiae with ice-cold PBS. Cells were cultivated in flasks containing DMEM/F-12 supplemented with 10% fetal bovine serum (FBS) and 1% penicillin/streptomycin.

Streptozotocin (STZ) was purchased from Wako Pure Chemicals (Osaka, Japan). Terudermis was used as an artificial dermis and kindly provided by Olympus Terumo Biomaterials Corporation (Tokyo, Japan).

2.2 *Isolation and Culture of Mesenchymal Stromal Cells*

Rat BMCs were harvested by flushing femurs and tibiae with ice-cold phosphate-buffered saline (PBS) as previously described.[21] Cells were filtered through a 70-μm nylon mesh and plated in T75-cm^2 or T225-cm^2 flasks with DMEM/F-12 (Gibco, Grand Island, New York) supplemented with 10% fetal bovine serum (FBS) and 1% penicillin/streptomycin. The cultures were kept in a humidified atmosphere containing 5% CO_2 and 95% air at 37 °C. Nonadherent cells were removed after 24 h. Adherent cells were trypsinized with 0.25% trypsin-EDTA (Gibco), harvested, and then plated into new flasks at every 90% confluency. Adherent cells from passage 2 were frozen in liquid nitrogen for future use. Early passage cells were examined for their capacity to differentiate in culture (Fig. 1).

2.3 *In-Vitro Differentiation Assay*

Passage 4 MSCs were tested for their ability to differentiate into osteocytes and adipocytes. For adipocyte differentiation, cells (2×10^5) were cultured with Differentiation Media BulletKits-Adipogenic (Lonza, Basel, Switzerland) according to the manufacturer's instructions. MSCs were cultured in six-well plates with MSCs culture medium until they reached confluency. Cells were then exposed to three cycles of adipogenic induction media alternating with adipogenic maintenance media. Following three complete cycles of induction/maintenance, the MSCs were cultured for 7 more days in supplemented adipogenic maintenance medium. Cell differentiation to adipocytes was confirmed by Oil Red O (Muto Chemicals, Tokyo, Japan) staining. For osteogenic differentiation, cells (2×10^4) were plated, and the culture medium was replaced with Differentiation Media BulletKits-Osteogenic (Lonza) until confluence. Cells were stained with alizaline red S (Wako Pure Chemicals).

2.4 *Diabetic Wound Model and Cell Transplantation*

To induce diabetes mellitus, streptozotocin (STZ) in a 0.1-M citrate buffer (pH 4.3) was injected intravenously into the penile vein of normal LEW rats (60 mg/kg body weight). Rat blood glucose levels were then assessed using a glucometer after 3 days, and individual rats with glucose levels greater than 250 mg/dl were classified as diabetic and immediately utilized for further experimentation.

STZ-induced diabetic rats were anesthetized with pentobarbital (40 mg/kg) and full-thickness skin defects (2×2 cm) were made on the scalp.[22] Two hundred microliters of PBS containing fresh BMCs (1×10^7) or MSCs (1×10^7) was added to the inner layer of the same-sized artificial dermis for 30 sec at room temperature.[23] The wound was covered with the impregnated artificial dermis and sutured using 4-0 nylon. Artificial dermis impregnated with PBS was grafted onto rats that formed the control group.

The wounds were photographed every week in a standard prone position, and were monitored by planimetry using Scion image software (Scion Image Alpha 4.0.3.2, Scion Corporation, Maryland). The percent of wound area was calculated as the ratio of the nonhealing wound area to the original wound area.

2.5 *In-Vivo Bioluminescent Imaging*

In-vivo luminescent imaging was obtained using the noninvasive bioimaging system IVIS™ (Xenogen, Alameda, California) and analyzed using Igor (WaveMetrics, Lake Oswego, Oregon) and IVIS Living Image (Xenogen) software packages. To detect luminescence from luciferase-expressing cells, D-luciferin (potassium salt, Biosynth, Postfach, Switzerland) was injected intravenously into the penile vein or subcutaneously into the head skin of rats anesthetized (30-mg/kg body weight) with isoflurane. The signal intensity was quantified as photons flux in units of photons/sec/cm^2/steradian in the region of interest.

2.6 *X-Gal Staining and Immunohistochemistry*

Rats were euthanized and the systemic circulation was flushed through the left ventricle with PBS followed by 4% paraformaldehyde (PFA). Specimens were divided and fixed in 4% PFA, and embedded in either paraffin or Tissue Tec OCT Compound (Sakura Finetechnical Company, Limited, Tokyo, Japan). Thin sections (4 to 7 μm) were stained with hematoxylin and eosin, or were used for immunohistochemistry.

To visualize lacZ expression, X-gal staining was performed as previously described.[18] Briefly, sections were washed three times with PBS containing 2-mM $MgCl_2$, 0.01% sodium deoxycholate, and 0.02% Nonidet-P40. Specimens were treated with a β-gal staining solution (1 mg/ml of 5-bromo-4-chloro-3-indolyl-b-D-galactopyranoside, 2-mM $MgCl_2$, 5-mM potassium hexacyanoferrate [III], and 5-mM potassium hexacyanoferrate [II] trihydrate) at 37 °C for 1 to 2 h.

For immunohistochemistry, sections were probed with anti-CD31, anti-VEGF, and anti-HIF-1α antibodies. Specimens were blocked with 1% BSA in PBS and incubated overnight at 4 °C with anti-CD31 (diluted 1:50, 4 μg/ml), anti-VEGF (diluted 1:100, 100 μg/ml), and anti-HIF-1α antibody (diluted 1:200, 5 μg/ml), in 0.1% BSA, respectively. Biotinylated antirabbit IgG (Vector Laboratories, Burlingame, California) or biotinylated antimouse IgG (Vector Laboratories) was used as the secondary antibody (diluted 1:200 in 0.1% BSA for 1 h at room temperature). The labeled sections were incubated with horseradish peroxidase (HRP)-conjugated streptavidin (Vector Laboratories), and followed by diaminobenzidine (0.5 μg/ml) for color visualization. Specimens were counterstained with hematoxylin. In sections stained with anti-CD31 antibody, CD31-positive tubular structures within the wound were considered as blood vessels. In ten similar sections, CD31-positive vessels were counted and normalized to 1 mm.[24]

2.7 *Statistical Analysis*

The Student's t-test, Tukey's HSD test, and U-test were used for the statistical analyses. The SPSS 11.0 system (SPSS Incorporated, Chicago, Illinois) was used for the statistical analysis. Differences between groups were considered significant when $P<0.05$.

3 Results

3.1 *Characteristics of Bone-Marrow-Derived Mesenchymal Stromal Cells from Transgenic Rats*

To define the isolated MSCs from adult transgenic rats, the expression of cell surface markers was examined using FACS analysis [Fig. 2(a)]. As previously described,[5,10] isolated MSCs from lacZ-transgenic rats[18,19] were CD29 and CD90 (Thy-1) positive, and CD34 and CD45 negative. Moreover, the MSCs rapidly proliferated, formed colonies, and retained an adherent spindle-shaped morphology [Fig. 2(b)]. These cells were capable of differentiating into adipocytes [Fig. 2(c)] and osteocytes [Fig. 2(d)]. All of these phenotypes were equivalent to those of wild-type rats, and remained unchanged even in luciferase transgenic rats (data not shown). Thus, these results demonstrate that MSCs from transgenic rats possess appropriate differentiation potential. To avoid loss of multipotentiality for differentiation through passage in culture, MSCs derived from no more than a fourth passage were used for all experiments.

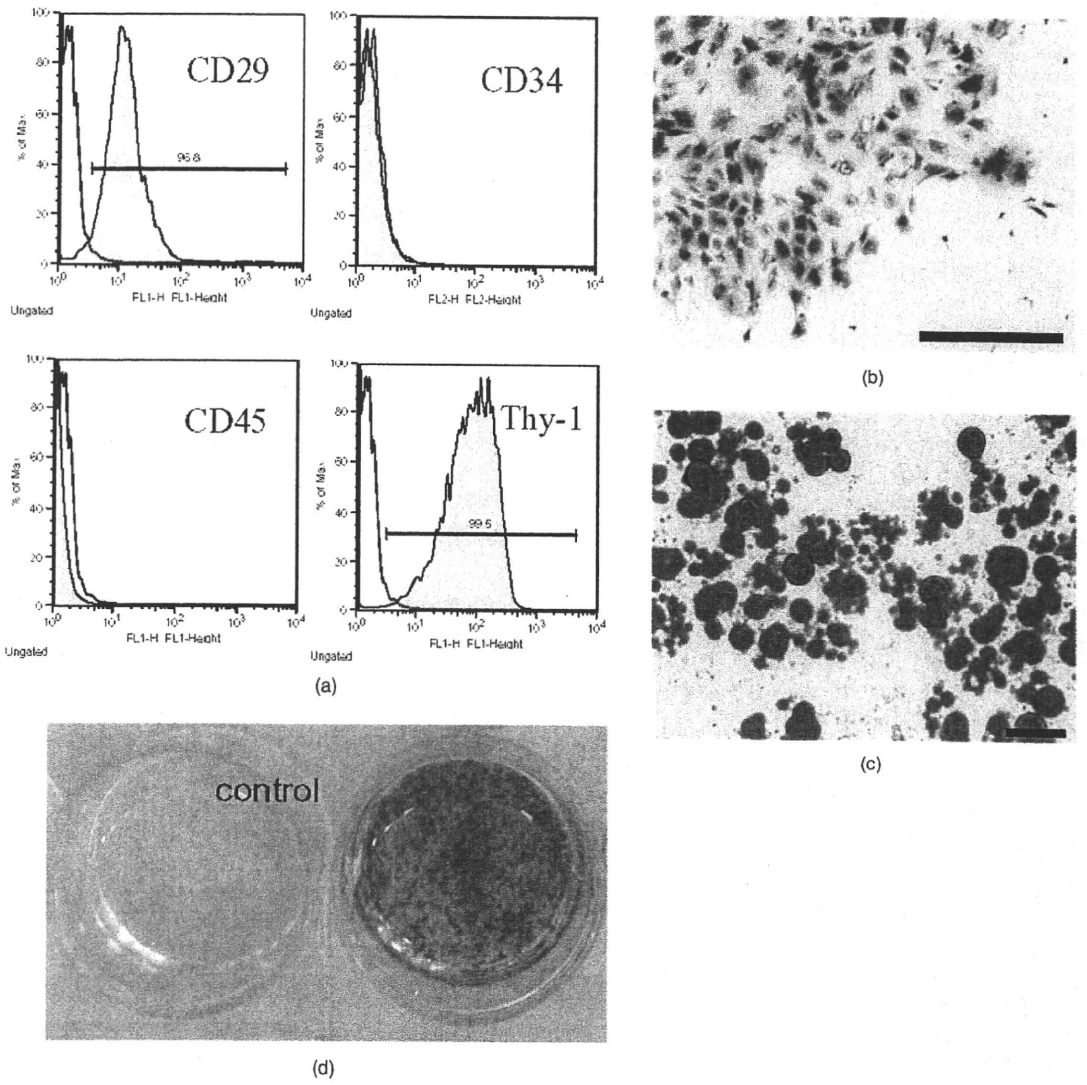

Fig. 2 Characteristics of MSCs. (a) Flow cytometric histogram analysis of culture-expanded MSCs was performed as detailed in Sec. 2. Expression profiles for CD29, CD34, CD45, and Thy-1 are depicted. Cells were uniformly negative for CD34 and CD45, and positive for CD29, Thy-1 markers associated with MSCs. Specific antibody profile (gray) versus isotype-matched antibody control (black line) is shown. (b) Colony formation of MSCs from wild-type LEW rats. Colonies were stained with crystal violet. Adherent spindle-shaped cells proliferated to form colonies. Bar = 500 μm. Under appropriate differentiation conditions, MSCs were capable of differentiating into (c) adipocytes (stained with Oil Red O for lipid droplets; Bar=50 μm) and (d) osteocytes (stained with alizaline red for mineral deposition).

To visualize the fate of MSCs, luminescence sensitivity was examined in luc-Tg-derived MSCs. As shown in Fig. 3(a), at least 5×10^4 MSCs from luc-Tg rats are required for substantial detection over the background *in vitro*, even though a linear dose-dependent output of light was maintained in the presence of D-luciferin. Although the MSCs comprised approximately 0.001% freshly isolated BMCs (data not shown), both expanded MSCs in culture and freshly isolated BMCs exhibited equivalent photon counts at the same cell number (1×10^6) [Fig. 3(b)].

3.2 *Topical Administration of Mesenchymal Stromal Cells Promotes Skin Wound Healing in Diabetic Rats*

To investigate whether skin wound healing could be impaired in the diabetic condition, streptozotocin (STZ) was intravenously injected into the penile vein of male rats, and full-thickness skin defects (2×2 cm) were then made on the scalp of diabetic rats (greater than 250 mg/dl of blood glucose). The skin defect was covered with an artificial dermis.

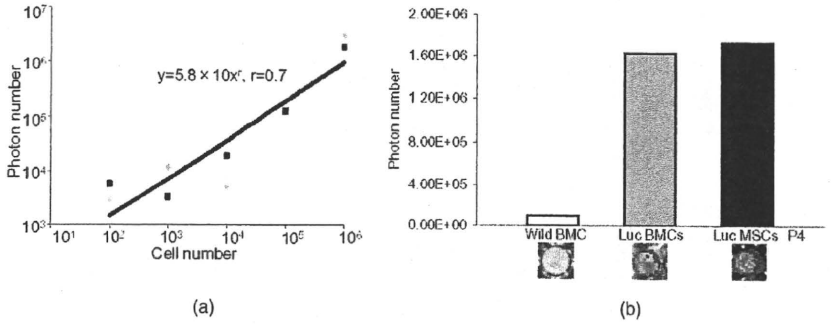

Fig. 3 Characteristics of MSCs from luciferase Tg LEW rats. (a) Luciferase activity of MSCs from luciferase Tg LEW rats. MSCs from luciferase Tg rats were plated onto 96-well plates at the indicated number. Luciferase activity (photon intensity) was evaluated in the presence of D-luciferin. Data represent the mean luciferase activity from two independent experiments (black squares and gray diamonds represent two different experimental trials). (b) Luciferase-expressing BMCs and MSCs possessed stronger luciferase activity than wild-type BMCs.

The wound area of diabetic rats was significantly smaller than that of control rats [Figs. 4(a) and 4(b)]. Skin wounds of control rats were almost totally restored at 3 weeks, while those of diabetic rats remained unhealed. These findings indicate impaired wound healing in diabetic rats.

In an effort to address the therapeutic effect of MSCs on skin wounds in diabetic rats, skin defects of diabetic rats were treated with either MSCs or BMCs that were impregnated within an artificial dermis. Since an artificial dermis provides a scaffold for tissue regeneration and is amenable to impregnation with various cellular materials, it was used as a scaffold for the MSCs and BMCs. As shown in Figs. 5(a) and 5(b), the wound area of MSC-treated diabetic rats was strikingly smaller than that of BMC-treated diabetic rats 1 week after treatment. Notably, retention of MSCs and BMCs in the wound site was difficult without the artificial dermis (data not shown). These data demonstrate that topical administration of MSCs promotes skin wound healing in diabetic rats at an early stage. The artificial dermis promoted wound healing at 2 and 3 weeks after treatment, although the artificial dermis when used with BMCs or MSCs was not significantly smaller than when it was used alone.

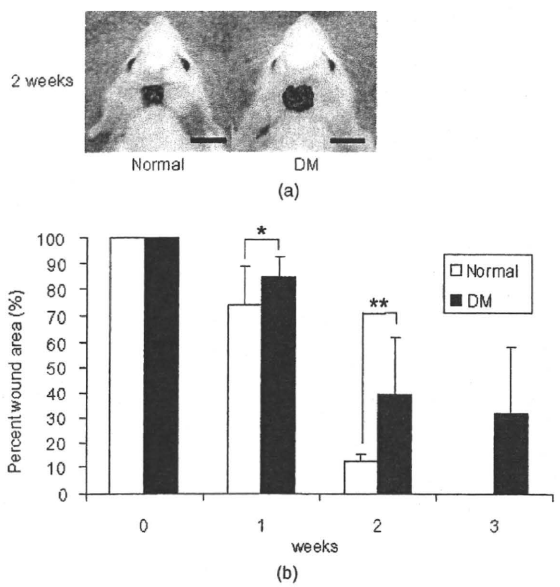

Fig. 4 Delayed wound healing studies in rats. A square area (2 × 2 cm) was surgically excised down to muscle fascia on the head of streptozotocin (STZ)-induced diabetes mellitus (DM) LEW rats or normal LEW rats (n=22 animals in total). (a) The wounds were photographed every week, followed by planimetry analysis using Scion image software. Bar=1 cm. 1 and 2 weeks after the operation, DM rats healed significantly more slowly (b) than normal rats ($^{*}p<0.05$ and $^{**}p<0.01$, respectively). The skin wounds of normal rats were totally restored at 3 weeks. Data expressed as means ±SD. DM stands for streptozotocin-induced diabetes mellitus LEW rats. Normal is for normal LEW rats.

3.3 *Fate of Topically Administered Mesenchymal Stromal Cells on the Skin Wound of Diabetic Rats*

To examine the fate of MSCs administered topically onto the wound area of diabetic rats, either MSCs or BMCs from luc-Tg rats were used as the therapeutic cell source with an artificial dermis. As shown in Fig. 6(a), MSC-derived photons were obtained during the whole period of wound healing (for 21 days), although photon counts decreased within a few days [to 40%, Fig. 5(b)]. BMC-derived photons decreased considerably to background levels within 7 days [Fig. 6(b)]. These results demonstrate that MSCs administered topically were retained to a greater extent than BMCs at the wound area of diabetic rats.

3.4 *Mesenchymal Stromal Cells Accelerate Angiogenesis during Diabetic Wound Healing*

Since the wound area of MSC-treated diabetic rats improved 1 week after treatment, specimens were stained with hematoxylin and eosin. As shown in Fig. 7(a), an increased number of vessel structures was observed in the MSC specimen, suggesting neoangiogenesis. Neoangiogenesis is a critical step in wound healing, and the CD31 molecule represents a major marker for vascular endothelial cells. Therefore, we set out to determine whether the administered MSCs affected the CD31-positive vessel number at the wound site of diabetic rats. In contrast with BMC treatment, MSC treatment showed that

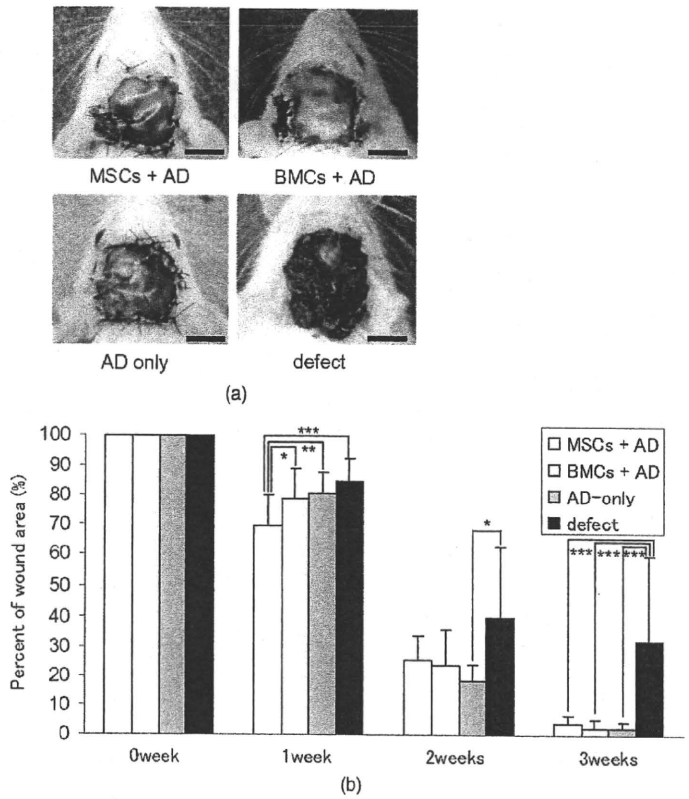

Fig. 5 Healing effect of MSCs on diabetic wounds. (a) Groups comprising MSCs+artificial dermis (AD), BMCs+AD, AD-only, and defects were formed using DM rats (n=58 animals in total) and photographed 1 week after transplantation. Bar=1 cm. (b) Percent of wound area was calculated using Scion image software, and values for the MSCs+AD group were significantly lower than those for the BMCs+AD, the AD-only and defect groups at 1 week after transplantation (*$p<0.05$, **$p<0.01$, and ***$p<0.001$, respectively). Data expressed as means ±SD.

CD31-positive adventitial vessels significantly increased in number at 1 week posttreatment ($p<0.001$) [Fig. 7(a)]. Furthermore, MSCs from LacZ-Tg rats were used to assess the relationship between the presence of MSCs and vascular endothelial growth factor 1 (VEGF-1) expression using immunohistochemistry [Fig. 7(b)]. Specimens were stained using anti-VEGF antibodies and X-gal 1 week following cell transplantation. In comparison with BMC treatment, MSC transplantation increased VEGF expression with LacZ-expressing cells. Expression of hypoxia-inducible factor 1α (HIF-1α), whose transcription factor tightly regulates VEGF expression under hypoxic conditions, was also well correlated with VEGF expression [Fig. 7(b)]. These results suggest that HIF-1-mediated VEGF expression contributes to the increased number of vessels at the wound site.

4 Discussion

It has long been known that BMCs are mobilized during wound healing with inflammatory cells to orchestrate a cascade of tissue repair events.[25] Green fluorescent protein (GFP)-labeled bone marrow transplantation in wild-type mice allowed Badiavas et al. to demonstrate the participation of BMCs in cutaneous wound healing.[26] In this study, we demonstrated that the transplantation of MSCs enriched from BMCs significantly decreased the wound area in a diabetic rat model, and that prolonged presence of MSCs was correlated with wound healing.

In addition to the differentiation potential, MSCs can easily be isolated and transferred from the laboratory to the bedside. Once expanded, MSCs in a culture from the patient could be stored under appropriate temperature conditions before use, and therefore MSCs from the same donor could be transplanted repeatedly.[27] Furthermore, recent advances in gene transfer technology also allow for transient or stable modification of MSCs (to produce a particular cytokine).[28,29] These attractive features of MSCs encourage the use of MSCs as therapeutic tools and for cell therapy. The presence of MSCs accelerated greater angiogenesis than BMCs, suggesting that MSCs are more effective than BMCs.

In this study, we used an artificial dermis to retain MSCs at wound sites. Artificial dermal substitutes are structurally optimized to incorporate the surrounding tissue and promote subsequent dermal remodeling.[7,23] Many types of dermal substitutes for wound coverage have been developed and are currently available.[30–33] Collagen matrix substitute dermis or artificial dermis is feasible for skin defects and is now commercially available for deep wounds, in which bones and/or tendons are exposed.[30–32] The use of an artificial der-

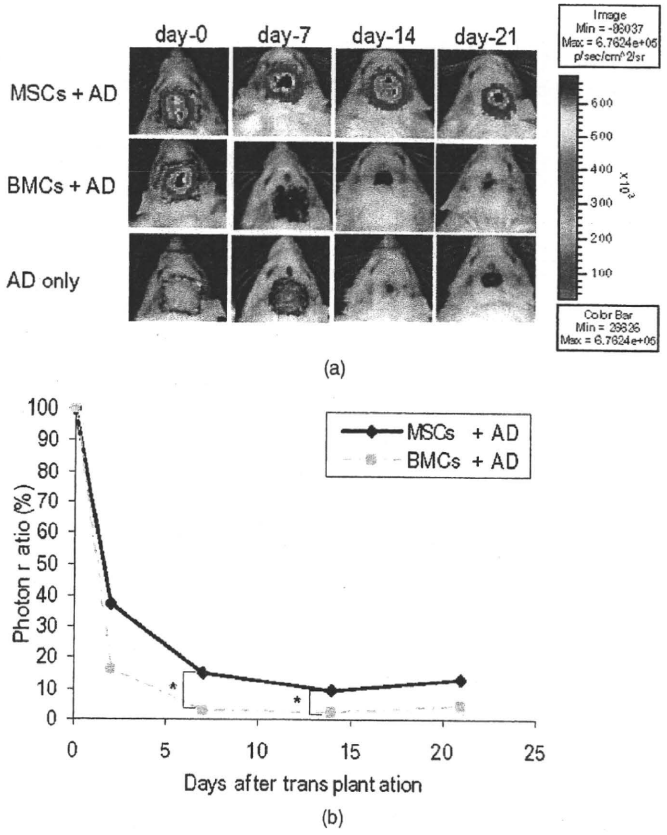

Fig. 6 Transplantation of artificial dermis-impregnated luciferase-expressing bone-marrow-derived cells. Groups comprising MSCs+AD, BMCs +AD, and AD-only were formed using DM rats (n=15 animals in total). D-luciferin was injected locally into the head skin of rats and luminescence was detected using the IVIS system. (a) Luminescence was recorded 0, 7, 14, and 21 days post-transplantation. (b) The time-course rate of luminescence is depicted. The MSCs+AD group had significantly higher luminescence than the BMCs+AD group (*$p<0.05$).

mis provides a scaffold for tissue regeneration, in which sprouting capillaries and fibroblasts are capable of migrating into the collagen matrix. In this study, it was necessary for a scaffold to retain MSCs and BMCs in the wound site. The artificial dermis could easily be impregnated with various cellular material, and therefore their combination is expected to significantly improve the healing of chronic skin ulcers caused by ischemic disease, venous insufficiency, and diabetes.

In vivo luminescent imaging showed that prolonged retention of transplanted MSCs at the wound site was correlated with healing and an increased number of vessels. Prior to characterization being based on potential differentiation, MSCs were characterized based on criteria that included the ability to adhere to tissue culture plates, resemblance to fibroblasts *in vitro*, and colony formation.[34] Therefore, we assume that retention of MSCs at wound sites may be associated with their adhesion properties. In fact, Pittenger et al. demonstrated integrin expression with MSCs and noted the presence of alpha 1, alpha 2, alpha 3, alpha a, alpha v, beta 1, beta 3, and beta 4, together with other adhesion molecules such as ICAM-1, ICAM-3, VCAM-1, ALCAM, and endoglin/ CD105.[10] Moreover, Ruster et al.[35] also demonstrated the expression of beta1 integrin VLA-4/CD49d on approximately 50% of the MSCs population present, and that MSCs are capable of rolling and adhering to cells that line blood vessels *in vitro* and *in vivo* in a P-selectin- and VLA-4/ VCAM-1-dependent manner. Thus, the aforementioned supporting evidence allows us to speculate that the adhesion potential in MSCs can contribute to the observed retention at wound sites. In addition to the MSCs character, the improved wound healing associated with the use of MSCs may result from two possibilities. The first relates to the capacity of MSCs to secrete a variety of cytokines, which are relevant for tissue repair and regeneration.[36–38] These soluble mediators from implanted MSCs may complement early endogenous reactions that are involved in tissue repair, such as those involved in angiogenesis and extracellular matrix formation.[39] Treatment with MSCs resulted in enhanced expression of VEGF and an increased number of adventitial vessels, suggesting that MSCs contribute to angiogenesis. The second possibility may relate to the plasticity of MSCs to differentiate into a variety of cell types.[23] Since MSCs possess multidifferentiation potential, they may transdifferentiate into myoblasts and epithelium at the wound site.[22,23] However, the latter case is unlikely, since only a small number of transplanted MSCs were retained in

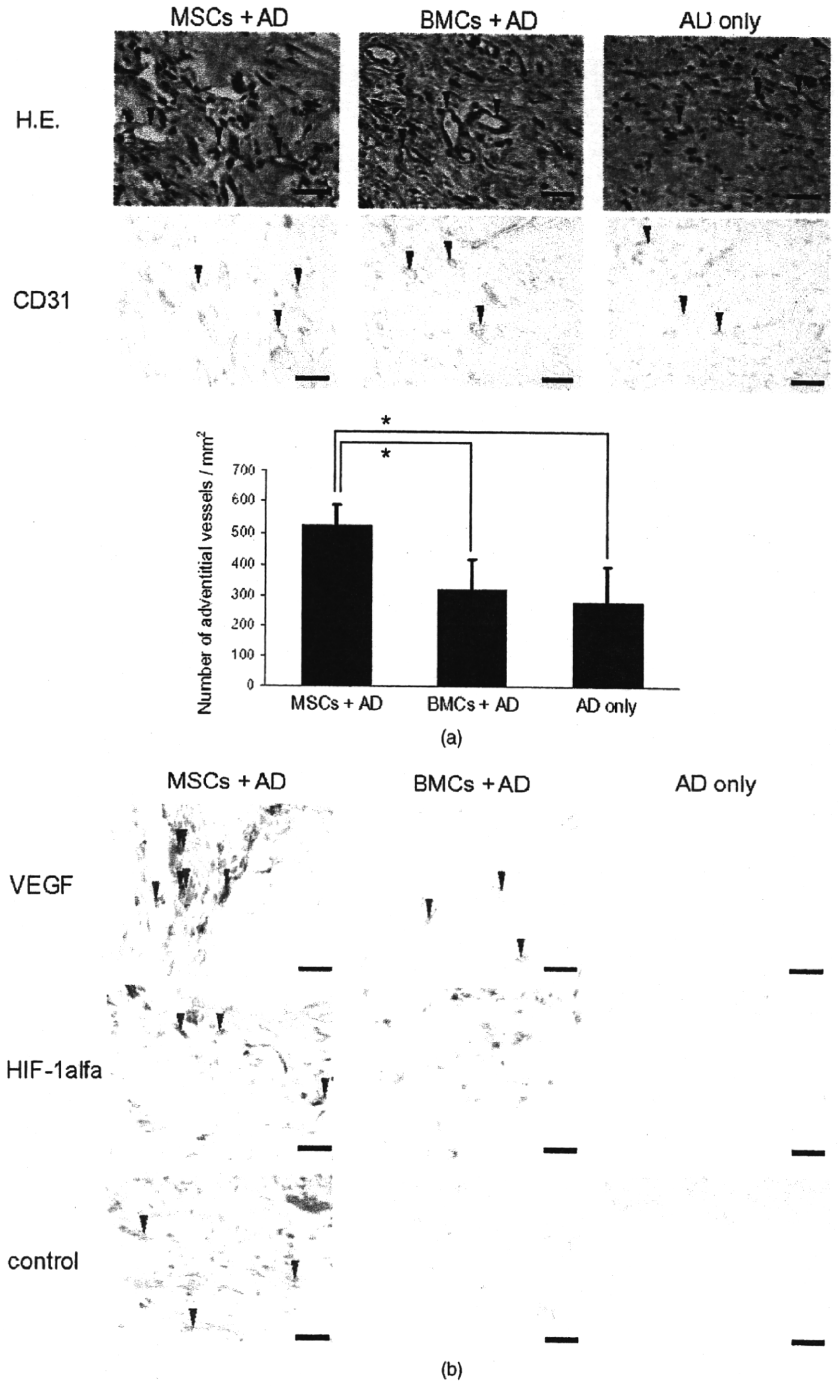

Fig. 7 Transplantation of artificial dermis-impregnated LacZ-expressing bone-marrow-derived cells. (a): Upper panels show hematoxylin and eosin (HE) staining at 1 week after the transplantation, and lower panels show CD31 immunostaining. Bar=20 μm. The MSCs+AD group had many microvessels (arrows) as shown by HE staining, and many CD31 positive vessels (arrows) as shown by CD31 immunostaining. The total vessel number was determined and expressed as vessel number/mm^2. The MSCs+AD group had significantly more vessels than the BMCs+AD and AD-only groups ($^*p<0.001$). Data expressed as means ±SD. (b) Specimens were stained for VEGF (red arrows), HIF-1α (yellow arrows), and mouse IgG (control) after X-gal staining (blue arrows). Bar=20 μm. The MSCs+AD group expressed considerable levels of VEGF and HIF-1α, and double-positive cells were identified.

the wound site, and MSC differentiation does not appear to be the major pathway for wound healing.

Since wound sites are relatively hypoxic, it was reasonable to record the expression of hypoxic condition-sensitive HIF-1α.[40] HIF-1α has been shown to stabilize and accumulate in cells under hypoxic conditions.[41] Interestingly, HIF-1α expression with MSC treatment was more enhanced compared with the control [Fig. 7(b)]. There is the possibility that exogenous MSCs stabilize or up-regulate HIF-1α, although this is difficult to determine due to the endogenous recruitment of MSCs.

In conclusion, the use of MSCs with an artificial dermis at an early stage could promote angiogenesis through MSC prolonged retention, and improve impaired wound healing in a diabetic rat model. To our knowledge, this is the first report to demonstrate the survival fate of transplanted MSCs in the diabetic condition, and to show that MSCs remained in the wound area, as determined by bioluminescent imaging. This preclinical model using MSCs provides an attractive strategy for cellular and scaffold therapies concerning intractable skin wounds such as diabetic wounds.

Acknowledgments

We would like to thank T. Yashiro, M. Kikuchi (Jichi Medical University), and all personnel in the Division of Organ Replacement Research, Center for Molecular Medicine, Jichi Medical University. We also wish to thank the Olympus Terumo Biomaterials Corporation for supplying the artificial dermis. This study was supported by grants from the Research on Health Sciences focusing on Drug Innovation program of the Japan Health Science Foundation (Kobayashi), and Research on Biological Resources (Murakami), Health of Labour Science Research Grants for Research from the Ministry of Health, Labour and Welfare, and the "High-Tech Research Center" Project for Private Universities: Matching fund subsidy from MEXT (Ministry of Education, Culture, Sports, Science, and Technology), 2002 to 2006. The transgenic rat embryos are available from the Health Science Research Resources Bank, National Bio Resource Project for the Rat, or Comparative Medicine Center and Research Animal Diagnostic Laboratory, College of Veterinary Medicine, University of Missouri, Missouri 65211.

References

1. N. Singh, D. G. Armstrong, and B. A. Lipsky, "Preventing foot ulcers in patients with diabetes," *JAMA, J. Am. Med. Assoc.* **293**(2), 217–228 (2005).
2. A. J. Boulton, L. Vileikyte, G. Ragnarson-Tennvall, and J. Apelqvist, "The global burden of diabetic foot disease," *Lancet* **366**(9498), 1719–1724 (2005).
3. Y. Yamaguchi et al., "Rapid healing of intractable diabetic foot ulcers with exposed bones following a novel therapy of exposing bone marrow cells and then grafting epidermal sheets," *Br. J. Dermatol.* **151**(5), 1019–1028 (2004).
4. Y. Wu, L. Chen, P. G. Scott, and E. E. Tredget, "Mesenchymal stem cells enhance wound healing through differentiation and angiogenesis," *Stem Cells* **25**(10), 2648–2659 (2007).
5. E. H. Javazon et al., "Enhanced epithelial gap closure and increased angiogenesis in wounds of diabetic mice treated with adult murine bone marrow stromal progenitor cells," *Wound Repair Regen* **15**(3), 350–359 (2007).
6. E. V. Badiavas and V. Falanga, "Treatment of chronic wounds with bone marrow-derived cells," *Arch. Dermatol.* **139**(4), 510–516 (2003).
7. S. Ichioka, S. Kouraba, N. Sekiya, N. Ohura, and T. Nakatsuka, "Bone marrow-impregnated collagen matrix for wound healing: experimental evaluation in a microcirculatory model of angiogenesis, and clinical experience," *Br. J. Plast. Surg.* **58**(8), 1124–1130 (2005).
8. V. Falanga, "Wound healing and its impairment in the diabetic foot," *Lancet* **366**(9498), 1736–1743 (2005).
9. Y. Misao et al., "Bone marrow-derived myocyte-like cells and regulation of repair-related cytokines after bone marrow cell transplantation," *Cardiovasc. Res.* **69**(2), 476–490 (2006).
10. M. F. Pittenger et al., "Multilineage potential of adult human mesenchymal stem cells," *Science* **284**(5411), 143–147 (1999).
11. M. B. Grant et al., "Adult hematopoietic stem cells provide functional hemangioblast activity during retinal neovascularization," *Nat. Med.* **8**(6), 607–612 (2002).
12. T. Asahara et al., "Isolation of putative progenitor endothelial cells for angiogenesis," *Science* **275**(5302), 964–967 (1997).
13. G. C. Kopen, D. J. Prockop, and D. G. Phinney, "Marrow stromal cells migrate throughout forebrain and cerebellum, and they differentiate into astrocytes after injection into neonatal mouse brains," *Proc. Natl. Acad. Sci. U.S.A.* **96**(19), 10711–10716 (1999).
14. K. W. Liechty et al., "Human mesenchymal stem cells engraft and demonstrate site-specific differentiation after in utero transplantation in sheep," *Nat. Med.* **6**(11), 1282–1286 (2000).
15. T. R. Brazelton, F. M. Rossi, G. I. Keshet, and H. M. Blau, "From marrow to brain: expression of neuronal phenotypes in adult mice," *Science* **290**(5497), 1775–1779 (2000).
16. E. Mezey, K. J. Chandross, G. Harta, R. A. Maki, and S. R. Mckercher, "Turning blood into brain: cells bearing neuronal antigens generated in vivo from bone marrow," *Science* **290**(5497), 1779–1782 (2000).
17. D. Woodbury, E. J. Schwarz, D. J. Prockop, and I. B. Black, "Adult rat and human bone marrow stromal cells differentiate into neurons," *J. Neurosci. Res.* **61**(4), 364–370 (2000).
18. H. Inoue et al., "Development of new inbred transgenic strains of rats with LacZ or GFP," *Biochem. Biophys. Res. Commun.* **329**(1), 288–295 (2005).
19. T. Murakami and E. Kobayashi, "Color-engineered rats and luminescent LacZ imaging: a new platform to visualize biological processes," *J. Biomed. Opt.* **10**(4), 41204 (2005).
20. Y. Hakamata, T. Murakami, and E. Kobayashi, "Firefly rats as an organ/cellular source for long-term in vivo bioluminescent imaging," *Transplantation* **81**(8), 1179–1184 (2006).
21. M. Takahashi et al., "Establishment of lacZ-transgenic rats: a tool for regenerative research in myocardium," *Biochem. Biophys. Res. Commun.* **305**(4), 904–908 (2003).
22. Y. Yamaguchi et al., "Bone marrow cells differentiate into wound myofibroblasts and accelerate the healing of wounds with exposed bones when combined with an occlusive dressing," *Br. J. Dermatol.* **152**(4), 616–622 (2005).
23. H. Nakagawa, S. Akita, M. Fukui, T. Fujii, and K. Akino, "Human mesenchymal stem cells successfully improve skin-substitute wound healing," *Br. J. Dermatol.* **153**(1), 29–36 (2005).
24. H. Yamashita et al., "Vasohibin prevents arterial neointimal formation through angiogenesis inhibition," *Biochem. Biophys. Res. Commun.* **345**(3), 919–925 (2006).
25. R. Gillitzer and M. Goebeler, "Chemokines in cutaneous wound healing," *J. Leukoc Biol.* **69**(4), 513–521 (2001).
26. E. V. Badiavas, M. Abedi, J. Butmarc, V. Falanga, and P. Quesenberry, "Participation of bone marrow derived cells in cutaneous wound healing," *J. Cell Physiol.* **196**(2), 245–250 (2003).
27. J. R. Mauney, V. Volloch, and D. L. Kaplan, "Role of adult mesenchymal stem cells in bone tissue engineering applications: current status and future prospects," *Tissue Eng.* **11**(5–6), 787–802 (2005).
28. M. Aluigi et al., "Nucleofection is an efficient nonviral transfection technique for human bone marrow-derived mesenchymal stem cells," *Stem Cells* **24**(2), 454–461 (2006).
29. L. Meinel et al., "Osteogenesis by human mesenchymal stem cells cultured on silk biomaterials: comparison of adenovirus mediated gene transfer and protein delivery of BMP-2," *Biomaterials* **27**(28), 4993–5002 (2006).
30. I. V. Yannas and J. F. Burke, "Design of an artificial skin. I. Basic design principles," *J. Biomed. Mater. Res.* **14**(1), 65–81 (1980).
31. R. Matsui, K. Osaki, J. Konishi, K. Ikegami, and M. Koide, "Evaluation of an artificial dermis full-thickness skin defect model in the rat," *Biomaterials* **17**(10), 989–994 (1996).

32. R. Matsui et al., "Histological evaluation of skin reconstruction using artificial dermis," *Biomaterials* **17**(10), 995–1000 (1996).
33. B. S. Atiyeh, S. N. Hayek, and S. W. Gunn, "New technologies for burn wound closure and healing--review of the literature," *Burns* **31**(8), 944–956 (2005).
34. A. J. Friedenstein et al., "Precursors for fibroblasts in different populations of hematopoietic cells as detected by the in vitro colony assay method," *Exp. Hematol.* **2**(2), 83–92 (1974).
35. B. Ruster et al., "Mesenchymal stem cells display coordinated rolling and adhesion behavior on endothelial cells," *Blood* **108**(12), 3938–3944 (2006).
36. M. Gnecchi et al., "Evidence supporting paracrine hypothesis for Akt-modified mesenchymal stem cell-mediated cardiac protection and functional improvement," *FASEB J.* **20**(6), 661–669 (2006).
37. T. Kinnaird et al., "Marrow-derived stromal cells express genes encoding a broad spectrum of arteriogenic cytokines and promote in vitro and in vivo arteriogenesis through paracrine mechanisms," *Circ. Res.* **94**(5), 678–685 (2004).
38. T. Kinnaird et al., "Local delivery of marrow-derived stromal cells augments collateral perfusion through paracrine mechanisms," *Circulation* **109**(12), 1543–1549 (2004).
39. A. T. Badillo, R. A. Redden, L. Zhang, E. J. Doolin, and K. W. Liechty, "Treatment of diabetic wounds with fetal murine mesenchymal stromal cells enhances wound closure," *Cell Tissue Res.* **329**, 301–311 (2007).
40. H. H. Hassanain et al., "Smooth muscle cell expression of a constitutive active form of human Rac 1 accelerates cutaneous wound repair," *Surgery (St. Louis)* **137**(1), 92–101 (2005).
41. S. Salceda and J. Caro, "Hypoxia-inducible factor 1alpha (HIF-1alpha) protein is rapidly degraded by the ubiquitin-proteasome system under normoxic conditions. Its stabilization by hypoxia depends on redox-induced changes," *J. Biol. Chem.* **272**(36), 22642–22647 (1997).

ELSEVIER

Journal of Autoimmunity 30 (2008) 163–171

journal of autoimmunity

www.elsevier.com/locate/jautimm

Review

In vivo bioimaging using photogenic rats: Fate of injected bone marrow-derived mesenchymal stromal cells

Mayumi Hara, Takashi Murakami, Eiji Kobayashi*

Division of Organ Replacement Research, Center for Molecular Medicine, Jichi Medical School, Tochigi 329-0498, Japan

Abstract

Mesenchymal stromal cells (MSCs) derived from bone marrow have the capacity for self-renewal and differentiation, and can give rise to cells of a muscle, bone, fat or cartilage lineage. Based on this potential and feasibility, MSCs are expected to be used in cell therapy for human diseases. Intriguingly, MSCs migrate to various *in vivo* locations, including injury and tumor sites. However, their cellular fate and distribution remain unclear. In this review, we first describe the potential of a photogenic transgenic rat that expresses fluorescent and/or luminescent proteins (e.g., green fluorescent protein and luciferase), and then focus on the characteristic migration of MSCs to injury and tumor sites. In addition, we will discuss an efficient delivery method for targeting the injured site. Synergized with modern advances in optical imaging, the photogenic rat system provides innovative preclinical tools and a new platform on which to further our understanding of matters concerning stem cell biology.

Keywords: Transgenic rat; Luciferase; Luminescent imaging; Chemokine receptors

1. Introduction

1.1. Transgenic rat system in regenerative medicine

The rat, as with the mouse, offers excellent animal models for biological and medical research, and has provided a wealth of physiological and pharmacological data. The larger body size of the rat in comparison to the mouse allows for the application of various physiological and surgical manipulations that may prove to have biological significance [1]. Since laboratory mice still represent a convenient experimental animal for research and monitoring the progression of genetic manipulations [2], the rat system may not have been regarded as a favorable model for biomedical research. However, new translational research fields in medicine (e.g., tissue engineering and regeneration medicine) demand the use of the rat system as an excellent animal model system, in which various techniques in medicine can be successfully applied. Recent advances in genetic manipulation have resulted in the development of the "color-engineered" rat system (see the review by Murakami and Kobayashi [1]).

Up to the mid-1990s, it was believed that only a limited number of organs and tissues possessed a regeneration program after birth. For example, repair in the adult brain was believed to be restricted to a post-mitotic event (see review by Hallbergson et al. [3]). However, current advances in regeneration medicine show promise for the restoration of form and function to damaged tissues. Mesenchymal stromal cells or mesenchymal stem cells (MSCs), which have been shown to differentiate into bone, cartilage, fat, myoblasts and neurons [4–9], are expected to be used in cell therapy for human diseases [10–12]. Although demonstration of functional tissue regeneration and the isolation of tissue precursor cells from adult organs have offered insights into a new therapeutic approach towards the repair of damaged tissues, knowing the fate of transplanted

Abbreviations: GFP, green fluorescent protein; Luc, luciferase; Tg, transgenic; LEW, Lewis; LacZ, beta-galactosidase; MHC, major histocompatibility complex; HSC, hematopoietic stem cell; MSC, mesenchymal stromal cell; SDF-1, stromal cell-derived factor-1; CXCL, CXC chemokine; CXCR, CXC chemokine receptor.

* Corresponding author. Division of Organ Replacement Research, Center for Molecular Medicine, Jichi Medical University, 3311-1 Yakushiji, Shimotsuke, Tochigi 329-0498, Japan. Tel.: +81 285 587 446; fax: +81 285 445 365.

E-mail address: eijikoba@jichi.ac.jp (E. Kobayashi).

0896-8411/$ - see front matter © 2007 Elsevier Ltd. All rights reserved.
doi:10.1016/j.jaut.2007.12.007

cells and tissues using appropriate markers is essential in delineating the scientific basis of such research. Therefore, the "color-engineered" rat system should play an important role in monitoring the *in vivo* fate of transplanted cells.

1.2. In vivo bioimaging for preclinical studies

In order to understand profound biological processes as they occur in living animals, imaging strategies have been developed and refined that reveal cellular and molecular biological events in real time. In particular, the development of molecular tags such as green fluorescent proteins (GFP) from the jellyfish (*Aequorea victoria*) and luciferase from the firefly (*Photinus pyralis*) has accelerated a revolution over the past decade, allowing complex biochemical processes to be associated with the functioning of proteins in living cells [13,14]. *In vivo* bioimaging utilizes fluorescent and/or luminescent proteins as internal biological light sources (e.g., GFP and luciferase), and offers important opportunities for the investigation of a wide variety of biological processes in living cells and animals [14,15]. Results from the application of these techniques are providing new and unique insights into biological processes occurring in the complex environment of the cell and/or the tissue. However, visualization of their fate needs an appropriate cellular marking procedure. Indeed, it is easy to use fluorescent dye and its use is relatively straightforward, but a significant drawback is that the fluorescent intensity decreases during *in vivo* cellular proliferation. Therefore, genetically encoded biological probes act as high-performance tools to visualize cellular fate in living animals.

2. Bone marrow-derived MSCs in rats

2.1. Characteristics of MSCs

The mammalian bone marrow is composed of two major types of stem cells, hematopoietic stem cells (HSCs) and non-hematopoietic stem cells. The latter stem cells are termed mesenchymal stromal cells or mesenchymal stem cells (MSCs) [16,17]. Mesenchymal cells are originally defined as primordial cells of mesodermal origin giving rise to skeletal muscle cells, blood, vascular and urogenital systems, and connective tissues throughout the body [16,18,19]. In this regard, MSCs have the potential for self-renewal and differentiation as exhibited by authentic HSCs, and based on their multi-lineage potential, MSCs are capable of differentiating into myoblasts, bone, cartilage or fat [4–9]. Thus, the clinical use of MSCs is of considerable interest in regenerative medicine.

Before the characterization of potential differentiation, MSCs were first described in the 1970s by Friedenstein et al. [20], who discovered that the cells adhered to tissue culture plates, resembled fibroblasts *in vitro*, and formed colonies. These characteristics have been identified in MSCs from numerous species, including humans, rats, mice and monkeys [21–25]. However, an issue of increasing importance concerning generation of MSCs is the lack of a specific marker or combination of markers that specifically define MSCs. It is known that *in vitro* expanded MSCs express phenotypically a number of non-specific markers, including CD105, CD73, CD90, CD166, CD44 and CD29 [4,26]. Hematopoietic and endothelial markers such as CD11b, CD14, CD31 and CD45 are generally negative [4]. Interestingly, although human and rat MSCs have been shown to be negative for CD34, both published and unpublished reports of murine MSCs demonstrate variation of CD34 expression [27–29]. MSC populations are often heterogeneous between species, and therefore it is necessary that generated MSCs are identified through a combination of physical, phenotypic and functional properties. The classical method used to identify MSCs is the colony forming unit (CFU) assay, in which adherent spindle-shaped cells that proliferate to form colonies should be identified and induced to differentiate into adipocytes, osteocytes and chondrocytes [16,18,19].

2.2. Generation of MSCs from photogenic rats

In an effort to obtain evidence in the laboratory for clinical applications, the performance of appropriate animal studies is one of the most critical steps. Based on the historical wealth and profound accumulation of physiological and pharmacological data, the rat system represents an important animal source for investigations concerning modern human health and medicine [1]. Cells from "color-engineered" rats are serving as unique cellular probes for modern biomedical research. As shown in Figs. 1A,B, isolated MSCs from wild-type LEW rats (MHC haplotype: $RT1^l$) exhibited typical adherent spindle-shaped cells that proliferate to form colonies, and differentiated into adipocytes (Fig. 1C) and osteocytes (Fig. 1D). An important question is "Do MSCs from engineered rats hold appropriate differentiation potential as previously defined by other research groups?" The answer is "yes", and the above characteristics were not altered even in transgenic rats that harbor a single reporter gene or double reporter genes (unpublished results). Figs. 1E–G demonstrate that MSCs from luciferase/lacZ and luciferase/GFP double transgenic rats hold their stable marker gene expression.

Based on clonal analysis within a given MSC population, only a low frequency of cells appear to have multi-potential differentiation with most of the cells [30]. There are also generally only a few clones capable of extensive expansion. Therefore, it is tempting to construct a hierarchical model regarding MSC cultures, in which multipotentiality for differentiation is lost through passage in a culture and the majority of cells become cells with a specific lineage potential. Senescence of typical MSC cultures is also frequently observed with progressive loss of multipotentiality. However, different MSC populations demonstrate varying propensities toward senescence. For example, human MSCs senesce after approximately 40 population doublings, whereas senescence of rat MSCs has not been reported [28,30]. Since MSCs from photogenic rats are also rapidly expanded into confluent cultures (unpublished results), this growth property appears to represent a common feature of rat MSCs even with genetic engineering.

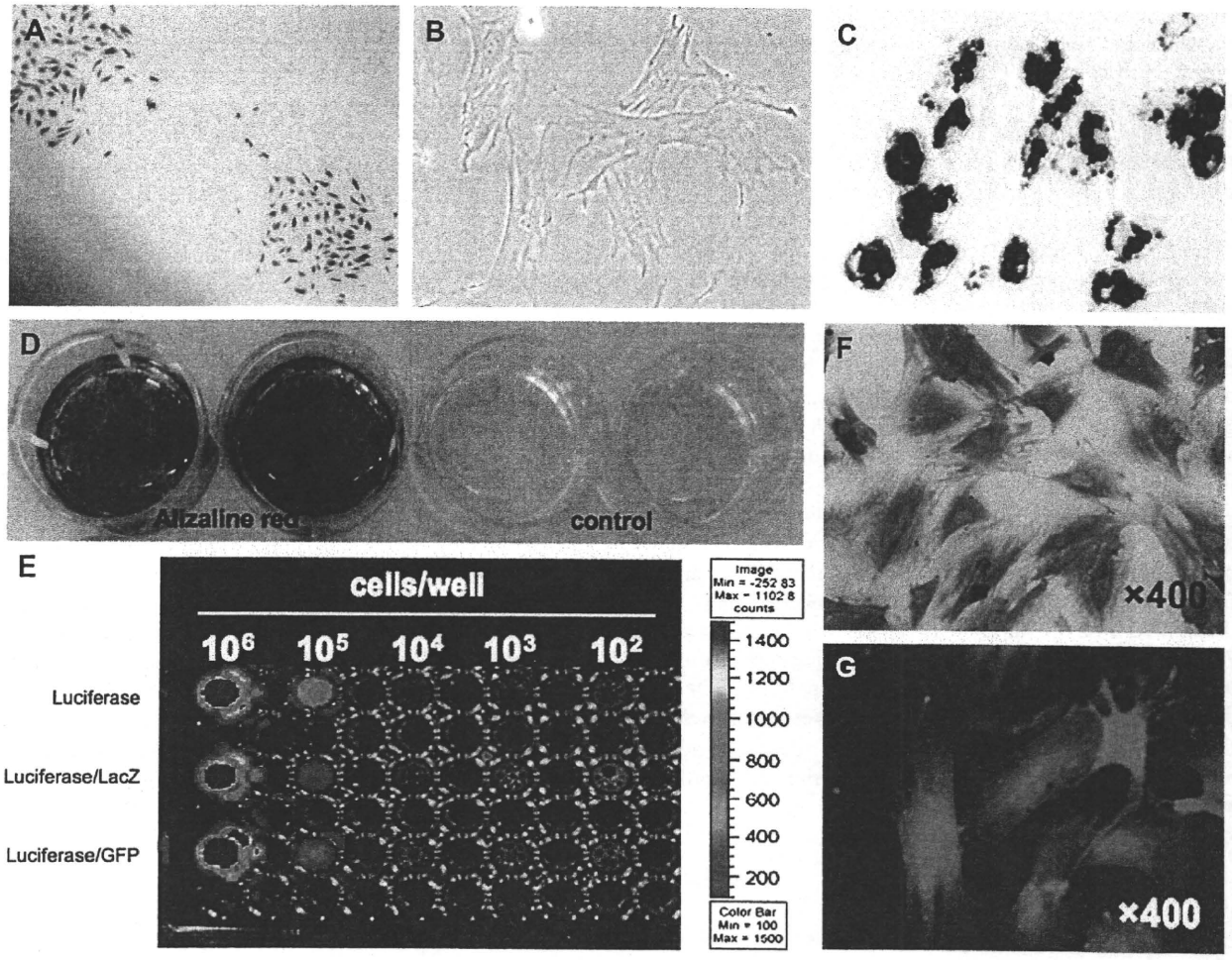

Fig. 1. Characteristics of MSCs from double reporter Tg LEW rats. (A) Colony formation of MSCs from wild-type LEW rats. Colonies were stained with crystal violet. Notably, adherent spindle-shaped cells proliferate to form colonies. (B) Morphologies of MSCs generated from wild-type LEW rats (original magnification ×400). Under appropriate differentiation conditions, MSCs were capable of differentiating into (C) adipocytes (stained with oil red O for lipid droplets; original magnification ×200) and (D) osteocytes (stained with alizaline red for mineral deposition). (E) Luciferase activity of MSCs from double reporter Tg rats. Luciferase/LacZ and luciferase/GFP double Tg LEW rats were created by cross-breeding luciferase Tg LEW rats [65] with LacZ and GFP LEW rats [66], respectively. Representative luciferase imaging is shown using IVIS™ (Xenogen, Alameda, CA). MSCs from luciferase/LacZ and luciferase/GFP double Tg LEW rats expressed (F) LacZ (by β-gal staining) and (G) GFP (under a 489-nm excitation light) (original magnification ×400).

3. Migration behavior of MSCs

3.1. Delivery of MSCs to the target tissue

MSCs possess a high expansion potential and genetic stability, and can be easily isolated and transferred from the laboratory to the bedside. These characteristics may provide a benefit for different delivery methods and formulations. Furthermore, MSCs have two other remarkable features: 1) the ability to migrate to sites of tissue injury and inflammation [31–33]; and 2) strong immunosuppressive properties that can potentially lead to successful autologous and heterologous transplantations [34]. In addition, MSCs have also been reported to migrate to tumors when they are systemically infused [35,36]. Thus, these attractive features of MSCs encourage investigation of MSCs as therapeutic tools and are leading us to potential uses for cell therapy.

Wakitani et al. [37] demonstrated MSC differentiation to myogenic cells *in vitro*, and also provided evidence that MSCs underwent myogenic differentiation in areas of induced muscle degeneration after infusion into immunodeficient mice [38,39]. However, although there is emerging evidence in regard to target migration and differentiation of MSCs through systemic injection [35,36,40,41], the fate of injected MSCs requires elucidation. Intravenously injected MSCs are mostly trapped in the microvasculature of the lung because of their size and the adhesion potential, and therefore it is not always thought to be the best route for MSC injection despite the migration potential of MSCs. A better method of MSC delivery may be through the artery [42,43]. We therefore investigated how MSCs from luciferase/LacZ double transgenic LEW rats migrate into a damaged limb muscle through the artery. Generated MSCs possessed an appropriate differentiation potential (see in Fig. 1), and MSCs (1×10^6) were injected

into either the right femoral artery or the muscle of LEW rats, in which the right hamstring muscle of rats was pretreated with 10 μM cardiotoxin (0.3 ml) to induce muscle degeneration [38]. MSC-derived photons were analyzed using *in vivo* luminescent imaging. As shown in Fig. 2A, MSC-derived photons could be easily observed at the injured site in the intra-arterial delivery, and signals of the intra-arterial delivery were 4–5 fold higher than those of the intramuscular injection. In fact, delivered cells in the muscle were clearly stained by beta-gal staining (Fig. 3B). These data strongly support the view that intra-arterial delivery of MSCs is potentially an efficient method for selective delivery to an injured site. We further examined the fate of increased numbers of MSCs (2.4×10^6) in the same animal model. Strikingly, the delivery method through the artery gave strong photo-signals at the injured limb site 30 min after infusion (day 0). However, data showed that MSC-derived photons were accumulated in the lung despite the injection of MSCs into the artery, suggesting that MSCs can potentially pass through peripheral capillaries. Moreover, the signals from the lung decreased within 2 days, whereas those from the injured limb did not increase and slowly faded out within 7 days. Thus, it is unlikely that recirculating MSCs after the pulmonary trapping migrate to the injured limb site. Although the intra-arterial delivery of MSCs is a worthy selective method for delivery towards injured sites, it should be noted that MSCs could pass through peripheral capillaries and be trapped in the lung.

3.2. Chemotactic migration of MSCs

The observation that infused MSCs accumulated at a tumor site [35,36,44] is of keen interest in the biology of MSCs (Fig. 4A). Indeed, the process of tumor stroma formation is similar to wound healing [45], and may result in tissue remodeling with a high proliferation of mesenchymal cells [46,47]. While the migratory behavior of MSCs has now been extensively reported, we have yet to determine what signal guides migration of MSCs to specific *in vivo* targets. If such a signal exists, what molecule mediates migration of MSCs? Inflammation at wound sites appears to be an initial signal, in which the homing and migration of leukocytes are promoted for the first defense through the deployment of chemokines and receptors. Chemokine receptors promote directional migration of immune cells toward inflamed tissues by inducing adhesion of leukocytes to endothelial cells through integrin activation, mediating cytoskeletal rearrangement to make cells more motile, and guiding cells in the direction of increasing chemokine gradients [48–50]. At present, many cell types, including smooth muscle, stromal, neuronal and epithelial cells, express chemokine receptors [51]. Thus, chemokines and their receptor system may be involved in multiple aspects of tissue homeostasis and cellular trafficking.

CXCL12 (stromal cell-derived factor-1 [SDF-1]) and its receptor CXCR4 play a critical role in homing, as shown by studies on engraftment of HSCs [52] and investigations of bone metastasis of breast and prostate cancer cells [53,54].

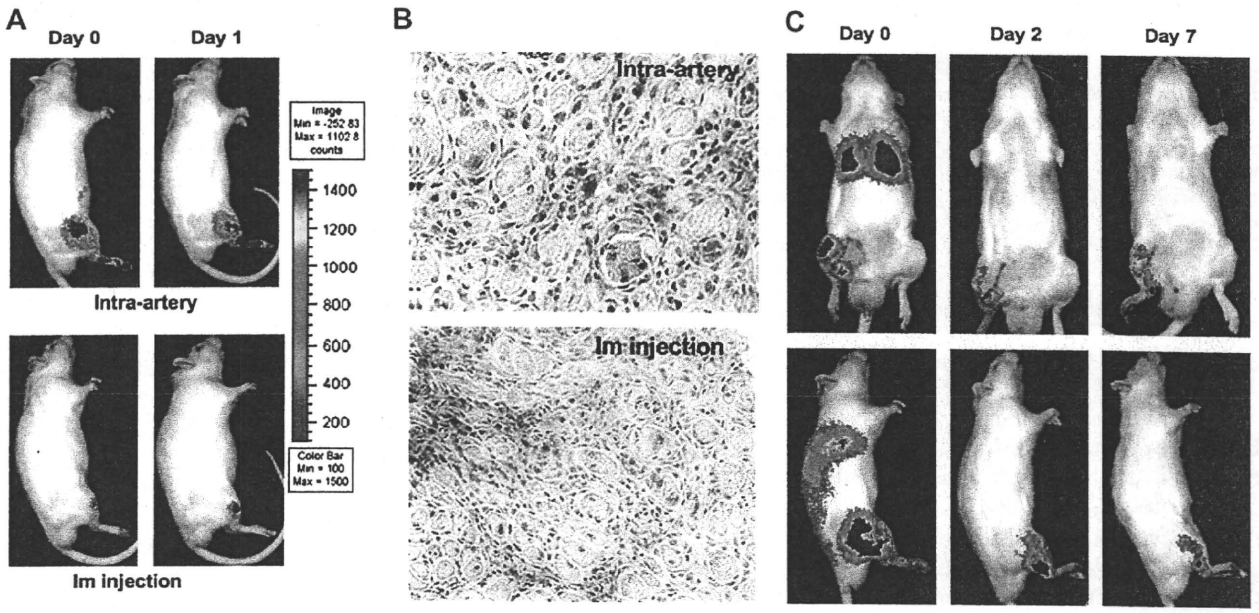

Fig. 2. *In vivo* luciferase imaging of injected MSCs from luciferase/LacZ double Tg LEW rats. (A) Degeneration of the right tibial muscle of LEW rats was induced by treatment with 0.3 ml of cardiotoxin (10 μM) 24 h before MSC injection. Luciferase/LacZ MSCs (1×10^6) were injected into either the right femoral artery (upper panels) or tibial muscle (lower panels) of muscle-injured rats, and MSC-derived photons were monitored using IVIS™ (Xenogen). (B) Accumulation of luciferase/LacZ MSCs in the injured muscle at 10 days post-injection (β-gal staining). Upper panel: MSCs injected through the femoral artery; lower panel: MSCs delivered through an intramuscular injection. Original magnification ×400. (C) Relatively higher number of luciferase/LacZ MSCs (2.4×10^6) injected into the femoral artery of rats pretreated with 10 μM cardiotoxin to induce muscle injury. Significant photons were observed in the lung and injured limb at day 0 post-injection (30 min).